Title: Sema3A Facilitates a Retrograde Death Signal via CRMP4-Dynein Complex Formation in ALS Motor Axons

Running Title: – Motor-Neuron Retrograde Death Signal.

Authors:

Roy Maimon[1], Lior Ankol[1], Romana Weissova[4,5], Elizabeth Tank[3], Tal Gradus Pery[1], Yarden Opatowsky[2], Sami Barmada[3], Martin Balastik[4], and Eran Perlson[1#]

Affiliations:

[1]Department of Physiology and Pharmacology, Sackler Faculty of Medicine, Tel Aviv University, Tel Aviv 69978, Israel

[2]The Mina and Everard Goodman Faculty of Life Science, Bar Ilan University, Israel

[3]Department of Neurology, University of Michigan, Ann Arbor, Michigan USA

[4]Institue of Physiology of the Czech Academy of Sciences, Prague, Czech Republic

[5]Faculty of Science, Charles University, Prague, Czech Republic

[#]**Corresponding Author:**

Eran Perlson, Ph.D., Dept. of Physiology and Pharmacology, Sackler Faculty of Medicine, Room 605, Sagol School of Neuroscience, Tel Aviv University, Ramat Aviv, Tel Aviv 69978, Israel. +972-3-6408743

eranpe@tauex.tau.ac.il

Key Words:

ALS, Retrograde Signaling, Human iPSC-Derived MNs, Axonal Transport, Sema3A

Abstract

Amyotrophic Lateral Sclerosis (ALS) is a fatal neurodegenerative disease with selective dysfunction; it causes the death of motor neurons (MNs). In spite of some progress, currently no effective treatment is available for ALS. Before such treatment can be developed, a more thorough understanding of ALS pathogenesis is required. Recently, we demonstrated that ALS-mutated muscles contribute to ALS pathology via secretion of destabilizing factors such as Sema3A; these factors trigger axon degeneration and Neuromuscular Junction (NMJ) disruption. Here, we focus on the molecular mechanism by which muscle contribute to MNs loss in ALS. We identified CRMP4 as part of a retrograde death signal generated in response to muscle-secreted Sema3A, in ALS-diseased MNs. Exposing distal axons to Sema3A induces CRMP4-dynein complex formation and MN loss in both mouse ($SOD1^{G93A}$) and human-derived (C9orf72) ALS models. Introducing peptides that interfere with CRMP4-dynein interaction in MN axons profoundly reduces Sema3A-dependent MN loss. Thus, we discovered a novel retrograde death signal mechanism underlying MN loss in ALS.

Summary

Maimon et al. identify a novel retrograde death mechanism that contribute to MN loss in ALS, in which CRMP4-Dynein complex is form and retrogradely move along the axon.

54 **Background**

55 Amyotrophic lateral sclerosis (ALS) is a lethal neurodegenerative disease that affects
56 upper and lower motor neuron (MN) health. This process leads to spasticity, muscle
57 atrophy, and paralysis, which develop into respiratory failure and patient death (Frey
58 *et al.*, 2000; Fischer *et al.*, 2004; Boillée, Vande Velde and Cleveland, 2006; Moloney,
59 de Winter and Verhaagen, 2014; Peters, Ghasemi and Brown, 2015). Currently, no
60 effective treatment exists for ALS, and finding basic mechanisms underlying the
61 progressive cell death is crucial. Although the cause of most ALS cases is unknown
62 (sporadic ALS-sALS), about 10% of ALS cases are inherited (familial ALS –fALS). The
63 most common mutations responsible for fALS include expansions of a repeated DNA
64 element (GGGGCC) in a gene termed *C9orf72*, and point mutations in the superoxide
65 dismutase 1 (SOD1) gene (Rosen *et al.*, 1993; DeJesus-Hernandez *et al.*, 2011;
66 Renton *et al.*, 2011). The $SOD1^{G93A}$ transgenic exhibit an ALS-like phenotype,
67 including axon degeneration, cytoplasmic inclusions, gliosis, loss of body weight, as
68 well as fatal upper and lower motor neuron deficits (Fischer *et al.*, 2004). However,
69 therapeutic success in the $SOD1^{G93A}$ mouse model, as well as other ALS mouse
70 models has not translated so far into an effective therapy. Thus, there is an urgent
71 need to use other more effective models. The use of human induced pluripotent stem
72 cells (iPSCs) from sporadic and familial ALS patients is a genetically precise and
73 promising approach for elucidating disease mechanisms and testing therapeutic
74 strategies. Indeed, in the past few years, multiple groups worldwide have
75 characterized iPSC-derived MNs that have recapitulated many aspects of ALS
76 pathology (Wen *et al.*, 2014; Alves *et al.*, 2015; Devlin *et al.*, 2015; Lee and Huang,
77 2017; Fujimori *et al.*, 2018; Shi *et al.*, 2018).

78

79 A hallmark finding in ALS models and humans with ALS is alterations in the axonal
80 transport process (Bilsland *et al.*, 2010; Perlson *et al.*, 2010; Gershoni-Emek *et al.*,

81 2015; De Vos and Hafezparast, 2017). MNs are highly polarized cells with long axons
82 that can reach 1 meter long in adult humans. In order to survive and function, MNs
83 depend on proper delivery of information and signalling events along the axons from
84 synapse to their soma (Harrington and Ginty, 2013; Millecamps and Julien, 2013;
85 Terenzio, Schiavo and Fainzilber, 2017; Zahavi, Maimon and Perlson, 2017). The
86 dynein/dynactin and kinesin motor protein families are responsible for retrograde and
87 anterograde axonal transport, respectively (Paschal and Vallee, 1987; Howard,
88 Hudspeth and Vale, 1989). Importantly, mutations in kinesin and dynein/dynactin are
89 associated with ALS in humans (LaMonte *et al.*, 2002; Münch *et al.*, 2004; Steinberg
90 *et al.*, 2015; Nicolas *et al.*, 2018). Several studies suggest that alterations in the cross
91 talk and long-distance signaling pathways between neurons and their diverse
92 extracellular cues, which are mediated by an axonal transport process, contribute to
93 ALS pathology (Boillée, Vande Velde and Cleveland, 2006; Perlson *et al.*, 2009; Gibbs
94 *et al.*, 2018).
95
96 Sema3A is a secreted protein that was initially identified because of its ability to induce
97 the collapse and paralysis of axonal growth cones of chick sensory neurons *in vitro*
98 (Luo, Raible and Raper, 1993). However, Sema3A has also been shown to induce
99 neuronal cell death via several mechanisms (Nakamura, Kalb and Strittmatter, 2000;
100 de Wit *et al.*, 2006; Ben-Zvi *et al.*, 2008; Yamashita *et al.*, 2014; Wehner *et al.*, 2016)
101 and to be involved in a variety of pathologies in adults, including ALS (Good *et al.*,
102 2004; De Winter *et al.*, 2006; Venkova *et al.*, 2014; Maimon *et al.*, 2018). Collapsin
103 Response Mediator Proteins (CRMPs) constitute a family well known for their
104 intracellular response to Sema3A-Plexin binding. There are 5 known CRMPs in
105 vertebrates, all of which share ~75 percent sequence similarities (Schmidt and
106 Strittmatter, 2007). The canonical signaling events of CRMPs during Semaphorin
107 signaling involve their phosphorylation via GTPase activity, which further leads to
108 microtubule destabilization and axon retraction (Sasaki *et al.*, 2002; Yamashita and

109 Goshima, 2012; Balastik *et al.*, 2015). In addition to their role in mediating Sema3A
110 intrinsic responses, CRMPs were also reported to bind dynein and kinesin, and
111 modulate their function (Arimura *et al.*, 2009; Rahajeng *et al.*, 2010). Several studies
112 further demonstrated the involvement of CRMPs in neurodegenerative diseases
113 (Charrier *et al.*, 2003; Yamashita and Goshima, 2012; Nagai, Baba and Ohshima,
114 2017). Specifically, CRMP4 expression levels were previously found to be elevated in
115 the SOD1^{G93A} mouse spinal cord, and were suggested to hamper MN health (Duplan
116 *et al.*, 2010; Valdez *et al.*, 2012; Nagai *et al.*, 2015). However, the mechanism underline
117 the involvement of CRMP4 mediating cell death and its role in other ALS model is still
118 elusive. Moreover, mutations in CRMP4 were associated with ALS patients (Blasco *et*
119 *al.*, 2013).
120
121 Here, we identified a novel retrograde death signal, triggered by Sema3A, which
122 facilitates MN loss in both murine and human ALS models. This process is mediated
123 by the formation of CRMP4-Dynein complex along diseased axons. Interfering with the
124 binding of CRMP4 to Dynein by using short blocking peptides rescues Sema3A-
125 dependent MN loss in these ALS models.
126
127 **Results**
128
129 **SOD^{G93A} MNs and muscle co-cultures enhance MN loss**
130 MN cell death is a key process in ALS pathology. Taking into consideration our
131 previous findings that muscle-dependent secretion of toxic factors can trigger axon
132 degeneration in MNs and accelerate SOD1^{G93A} MN loss (Maimon *et al.*, 2018), we
133 investigated whether muscle toxicity could also hamper MN cell survival. Similarly as
134 described before (Maimon *et al.*, 2018; Ionescu *et al.*, 2019), WT or SOD1^{G93A} P60
135 gastrocnemius muscles were dissected and cultured in the distal compartment of the
136 microfluidic chamber for 7 days. Then, WT$^{ChAT::tdTomato}$ or

137 SOD1$^{G93A/ChAT::tdTomato}$ explants were plated in the proximal compartment and grown
138 in the Micro Fluidic Chambers (MFC) until axons traversed into the distal
139 compartment and formed contact with the muscles. We tracked the number of
140 ChAT-positive MNs within spinal cord explants at this point (10DIV), and 5 days
141 after (15DIV) (Figure 1A-B). Our observations indicated that while under
142 WT$^{ChAT::tdTomato}$ conditions MNs survived, significant neuronal loss was observed
143 when SOD1$^{G93A/ChAT::tdTomato}$ explants were plated. Importantly, the MN loss was
144 enhanced in the presence of SOD1^{G93A} muscles (Figure 1C) (Mean: WT-WT 91.85
145 ± 3.673; SOD1^{G93A}-SOD1^{G93A} 69.24 ± 4.237; WT- SOD1^{G93A} 76.55 ± 2.575;
146 SOD1^{G93A}-WT 92.63 ± 3.047). Thus, although SOD1$^{G93A/ChAT::tdTomato}$ MNs are prone
147 to die, SOD1^{G93A} muscles also contribute to a more robust MN loss, suggesting
148 that both intrinsic and extrinsic mechanistic defects contribute to ALS.
149
150 **Sema3A activates a retrograde death signal in MNs of SOD^{G93A} mice**
151 As our previous report indicated, Sema3A is one of the toxic factors that are secreted
152 in excess by ALS-diseased muscles. We also found that Sema3A facilitates axon
153 degeneration and NMJ disruption (Maimon *et al.*, 2018). Sema3A were shown to be
154 involved in ALS also by other groups (De Winter *et al.*, 2006; Venkova *et al.*, 2014).
155 Here, we hypothesized that Sema3A will lead not only to MN axon degeneration, but
156 also to MN loss. To better understand this process, explants from WT embryos were
157 cultured and grown in the MFC until axons traversed into the distal compartment. At
158 this point, the retrograde tracer Alexa-647-conjugated Cholera Toxin Subunit B (CTX)
159 was added to the distal compartment in order to exclusively label the cell bodies of
160 neurons in the explant whose axons traversed into the distal compartment (Figure
161 1D). The number of CTX^{+} cells in the explant was quantified before, and then daily,
162 for one week, after Sema3A or its control medium was applied to the distal
163 compartment (Figure 1E). Our observations of WT explants did not indicate any
164 significant decrease in the number of cells (Figure 1E) (mean fold change over

165 control: Sema3A 0.95 ± 0.06; control 1 ± 0.05). However, applying Sema3A similarly
166 to explants from SOD1^{G93A} embryos resulted in a ~30% reduction of CTX^{+} cells as
167 early as after two days, compared with ~5% in the control (Figure 1F)(mean fold
168 change over control: Sema3A 0.68 ± 0.06; control 1 ± 0.04). Thus, despite inducing
169 the degeneration of both healthy and diseased MN axons, Sema3A affects survival
170 only in SOD1^{G93A} MNs.

171 Axonal transport is a process whereby cargo and signaling molecules are
172 moved efficiently to and from the MN peripheral axon; it is performed in the retrograde
173 direction by the dynein motor complex (Paschal and Vallee, 1987; Ibáñez, 2007;
174 Zahavi, Maimon and Perlson, 2017). Previous studies have also shown that Sema3A
175 can be internalized and undergoes retrograde transport to the soma (Dang, Smythe
176 and Furley, 2012; Yamashita *et al.*, 2014; Wehner *et al.*, 2016). It has also been shown
177 that Sema3A facilitates antero- and retrograde axoplasmic transport of organelles
178 (Goshima *et al.*, 1997). In order to determine whether Sema3A triggers MN loss in ALS
179 via a retrograde signaling event, we used an inhibitor for Dynein motor protein
180 (Ciliobrevin-D; hereafter Dyn-In) and thus blocked all retrograde transport events
181 (Movie 1-2). We repeated our experiments in the MFC with SOD1^{G93A} explants, but this
182 time Dyn-In was added to the distal compartment prior to Sema3A treatment (Fig 1F).
183 Importantly, inhibiting retrograde transport in the distal axon prevented MN loss in the
184 SOD1^{G93A} explant (mean fold change over control: Sema3A + Dyn-In 0.92 ± 0.09;
185 control 1 ± 0.04), indicating that Sema3A propagates cell death via a retrograde
186 signaling event. To further determine whether endocytosis of Sema3A components is
187 important for death signaling, as was shown before in different neurons (Wehner et al.,
188 2016), we applied Dynasore, a dynamin-dependent endocytosis inhibitor to the distal
189 axons prior to applying Sema3A, which was shown to internalize via this pathway
190 (Fournier *et al.*, 2000; Castellani, Falk and Rougon, 2004)(Movie 3-4)(Supplementary
191 Figure 1). Inhibiting Sema3A internalization did not rescue the MNs, and the number
192 of CTX^{+} cells was significantly reduced by ~30% after 2 days (Figure 1F)(mean fold

193 change over control: Sema3A + Dynasore 0.71 ± 0.01; control 1 ± 0.04). Hence, these
194 findings suggest that unlike in other types of neurons, Sema3A activates the retrograde
195 transport of a secondary messenger in order to facilitate MN loss, which is independent
196 of its internalization.
197
198 **C9orf72 patient-derived MN loss**
199 Human iPSC-derived MN cultures are currently widely used as an *in vitro* model in
200 studying ALS disease. Specifically, iPSC-derived MNs from individuals with *C9orf72*
201 mutations display several disease-relevant phenotypes, including abnormal
202 excitability and reduced survival (Devlin *et al.*, 2015; Sances *et al.*, 2016; Lee and
203 Huang, 2017; Shi *et al.*, 2018). We therefore plated human iPSC-derived MNs from
204 healthy controls and C9orf72-ALS patients in MFCs (Supplementary Figure 2 A-C).
205 Staining for the neuronal markers NFH and Tau, along with the MN-specific marker
206 HB9, validated the character of our cultures (Supplementary Figure 2 D-F). Here too,
207 we hypothesized that applying Sema3A to distal axons would trigger MN loss. To this
208 end, we applied the retrograde tracer Alexa-647-conjugated Cholera Toxin Subunit B
209 (CTX) after axons reached the distal compartment, labeling only the cell bodies of
210 MNs whose axons traversed into the distal compartment. The number of CTX^+ iPSC-
211 derived MNs was quantified before and 3 days after Sema3A was applied to the
212 distal compartment (Figure 1 G). We did not detect any significant loss of WT iPSC-
213 derived MNs in response to Sema3A, whereas *C9orf72* iPSC-derived MNs displayed
214 a 25 percent cell loss upon treatment with Sema3A (Figure 1 G-H). Hence, these
215 data suggest that Sema3A also triggers MN death in human iPSC-derived MNs
216 carrying the *C9orf72* mutation.
217
218 **CRMP4 levels are elevated in ALS models**
219 Our data indicate that Sema3A facilitates a downstream signaling event that
220 eventually forms a retrograde death signal in diseased MNs. Thus, we focused our

221 study on well-established Sema3A downstream effectors, the CRMP protein family.
222 The canonical signaling event by which CRMPs mediate the Sema3A repulsion effect
223 is via microtubule destabilization. Interestingly, CRMP4 levels were recently found to
224 be elevated in the SOD1^{G93A} spinal cord; this leads to MN cell death in unknown
225 mechanism. Moreover, a rare mutation in CRMP4 was found in a population of ALS
226 patients (Duplan *et al.*, 2010; Valdez *et al.*, 2012; Blasco *et al.*, 2013; Nagai *et al.*,
227 2015). Thus, we assumed that CRMP4 might be a key factor contributing to the
228 Sema3A-dependent MN loss that we observed. In order to verify that levels of
229 CRMP4 are indeed higher in SOD1^{G93A} sciatic nerve, we performed western blot
230 analysis and compared WT and SOD1^{G93A} P90 sciatic nerve (SN) extracts (Figure
231 2A). We found a significant elevation in CRMP4 expression in SOD1^{G93A} SNs,
232 compared with WT SNs (Figure 2B) (mean: WT 0.56 ± 0.11; SOD1^{G93A} 1.22 ± 0.14).
233 We further immunostained P90 sciatic nerves and searched for CRMP4 alteration
234 specifically in NF-H-positive axons (Figure 2C). We observed an increase in the
235 number of positive NF-H and CRMP4 colocalized areas per field (mean in μm^2: WT
236 1583 ± 478; SOD1^{G93A} 3015± 404) (Figure 2D). Our pervious data indicated that
237 SOD1^{G93A} SNs are exposed to higher Sema3A expression (Maimon *et al.*, 2018);
238 therefore, we assumed that CRMP4 will also be elevated *in vitro* after Sema3A
239 treatment in diseased MNs. We performed immunostaining in both healthy and
240 diseased human iPSC-derived MNs, and assessed the change in CRMP4 levels in
241 axons in the presence or absence of Sema3A. Our analysis revealed that indeed
242 CRMP4 intensity was increased only in diseased MNs treated with Sema3A (mean:
243 Healthy 0.7 ± 0.05; Healthy+Sema3A 0.75 ± 0.047; C9orf72 0.61 ± 0.03; C9orf72
244 1.27 ± 0.16) (Figure 2E-F). These results imply that intense Sema3A signaling may
245 drive the rise in CRMP4 levels in diseased MNs, and specifically in axons.
246
247 **CRMP4-dynein complex formation in ALS models**
248 In addition to mediating Sema3A signaling, CRMPs were previously reported to bind

249 motor proteins and modulate their function (Arimura *et al.*, 2009; Rahajeng *et al.*,
250 2010). Hence, we further hypothesized that elevated CRMP4 levels mediate MN loss
251 via its interaction with the motor protein dynein. We assumed that CRMP4-dynein
252 cross talk would be enhanced in MN axons of ALS models that were exposed to
253 Sema3A. To this end, we first extracted SN axoplasms from WT and SOD1^{G93A} P90
254 mice, and looked for CRMP4 that co-purified with dynein intermediate chain (DIC) via
255 immunoprecipitation. Strikingly, we observed a strong interaction of DIC with CRMP4
256 exclusively in the SOD1^{G93A} mice (mean: WT 0.28 ± 0.11; SOD1^{G93A} 1.48 ±
257 0.62)(Figure 3A-B). We next used the Proximity Ligation Assay (PLA) to validate our
258 result *in vitro*. As expected, we observed that indeed there is an increase in the
259 CRMP4-dynein colocalization along axons of the Sema3A-treated group, indicating
260 that Sema3A triggers this complex formation. Importantly, this colocalization was
261 twice as high in the SOD1^{G93A}-treated axons (Figure 3C-E). Next, we compared the
262 co-localized CRMP4-dynein puncta in human iPSC-derived MNs and observed
263 similar results. The CRMP4-dynein colocalization in *C9orf72* iPSC-derived MN axons
264 after Sema3A treatment was significantly higher compared with healthy control iPSC-
265 derived MN axons (mean puncta per axon: Healthy/control 5.4 ± 0.53;
266 C9orf72/Sema3A 10 ± 1.2) (Figure 3 F-G). Hence, we demonstrated both *in vivo* and
267 *in vitro* that CRMP4-dynein interaction increases in ALS-mutated MNs.
268 Since dynein is a retrograde motor protein, we expected that the dynein
269 interacting/cargo proteins would be retrogradely transported. We therefore assumed
270 that CRMP4 will change its localization and will move along the axon towards the cell
271 body. To better understand this process, we attempted to track exogenous CRMP4-
272 GFP movement in live cells, but overexpressing CRMP4-GFP resulted in a uniformly
273 defuse distribution. However, we hypothesized that endogenous CRMP4 would
274 demonstrate retrograde transport that could be identified by immunostaining distinct
275 cellular compartments (Olenick, Dominguez and Holzbaur, 2019). To this end, we

276 specifically examined CRMP4 levels in the cell bodies and proximal axons of MNs that
277 were distally exposed to Sema3A, Sema3A + Dyn-In, or control by using the same
278 CTX tagging approach as described before (Figure 3H). Similarly to what we have
279 previously shown, we observed that the levels of CRMP4 in proximal axons and cell
280 bodies were elevated by Sema3A treatment. Strikingly, inhibiting dynein completely
281 blocked the subsequent elevation of CRMP4 by Sema3A (mean: control 2± 0.2;
282 Sema3A 3 ± 0.1; Sema3A/Dyn-In 1 ± 0.01) (Figure 3I-J). Furthermore, we quantified
283 the cell body area for each treatment group and observed that Sema3A-treated MNs
284 exhibit smaller soma areas compared with control MNs. Here again, when Dyn-In was
285 added prior to applying Sema3A, this effect was abolished (mean: control 314± 10;
286 Sema3A 263 ± 10; Sema3A and Dynein inhibitor 318 ± 12) (Figure 3K). These data
287 indicate that the elevation in CRMP4 in the cell bodies and in proximal axons is indeed
288 mediated by dynein binding to axonal CRMP4 and subsequent retrograde transport of
289 the CRMP4-dynein complex.
290
291 **Specific peptides interfere with CRMP4-dynein interaction**
292 CRMP2 members were previously found to bind dynein motor protein (Arimura *et al.*,
293 2009). Arimura et al. also characterized two specific domains in CRMP2 protein,
294 which are responsible for dynein binding (Arimura *et al.*, 2009). Since CRMP2 and
295 CRMP4 share most of their sequence, we hypothesized that the CRMP2 dynein-
296 binding domains would play a similar role in CRMP4. Following this idea, and on the
297 basis of the CRMP4 protein crystal structure (PDB code 4CNT) (Ponnusamy *et al.*,
298 2014) (Figure 4A), we first examined if the same domains that are responsible for
299 CRMP2 dynein binding function similarly in CRMP4. To this end, we overexpressed
300 full length GFP-CRMP4 or CRMP4 missing amino acids 100-150 (GFP-ΔCRMP4) in
301 COS7 cells, and immunoprecipitated endogenous DIC. Western blot analysis of
302 these fractions revealed a strong interaction of DIC with full-length GFP-CRMP4 but
303 not GFP-ΔCRMP4 (Figure 4B-C)(mean: GFP-CRMP4 1.473± 0.373; GFP-ΔCRMP4

304 0.009± 0.001). Because a large truncation can result in CRMP4 misfolding and
305 dysfunction, we pursued a different strategy and blocked the association between
306 CRMP4 and dynein using small peptides modeled after the interaction domain. We
307 designed 4 peptides (CRMP4 Binding Peptides – CBP1-4) from within the 50 amino
308 acid domain with the potential to block the CRMP4-dynein interaction. Importantly,
309 the designed peptides' sequences are positioned away from the CRMP4 canonical
310 tetramer, and therefore are not likely to compromise activities related to the protein's
311 homomeric assembly (Figure 4A). Strikingly, pre-incubating a mixture of CBP1-4 with
312 lysate from GFP-CRMP4 overexpressing COS7 cells significantly reduced the
313 CRMP4-DIC interaction (Figure 4 B-C; mean: GFP-CRMP4 1.473± 0.373; GFP-
314 CRMP4 + Peptides 0.3± 0.05). We further examined the peptides' ability to block the
315 CRMP4-Dynein interaction in COS7 cells overexpressing Flag-tagged CRMP4. After
316 an overnight incubation of cell lysate with CBP1-4, we pulled-down Flag-CRMP4 and
317 blotted for dynactin (p150). Here again, application of the peptide mixture resulted in
318 a dramatic decrease in CRMP4 binding to dynein complex (mean: control 0.77± 0.1;
319 All Pep 0.17± 0.06) (Supplementary Figure 3A-B). We then determined whether
320 introducing individual peptides might be sufficient to block the CRMP4-Dynein
321 interaction. Using the same technique as before, we found that only CBP-4 had a
322 mild but significant ability to block CRMP4's interaction with dynactin (mean: control
323 1.92± 0.2; CBP1 1.44 ± 0.3; CBP2 1.34 ± 0.3; CBP3 1.8 ± 0.8; CBP4 1.13 ± 0.14)
324 (Supplementary Figure 3 C-D). Hence, although CBP-4 seems to be sufficient for
325 blocking CRMP4-Dynein binding, for achieving the optimal blocking of CRMP4-
326 dynein complex formation, a combination of all four peptides is required.
327 Since CRMP4 retrograde transport occurs in distal axons of MNs, we decided
328 to block CRMP4-dynein interaction specifically in MN distal axons. To this end, we
329 plated human iPSC-derived MNs in MFCs and introduced CBP1-4 into the distal
330 compartment comprised entirely of distal axons (Figure 4D). Using TAMRA peptides
331 as a positive control, we observed that CBP1-4 peptides were successfully taken up

332 by distal axons of MNs (Supplementary Figure 3 E-F). Strikingly, application of CBP1-
333 4 significantly interfered with the interaction of CRMP4 and dynein in distal *C9orf72*
334 iPSC-derived MN axons, but not control MN axons, as determined by PLA (mean:
335 C9orf72 8.9± 0.7; C9orf72 with Pep 1.6± 0.2) (Figure 4E). In light of these data, we
336 asked whether blocking the CRMP4-Dynein interaction in distal axons is sufficient to
337 rescue ALS-diseased MN death in response to Sema3A. Introducing the peptides into
338 diseased iPSC-MN axons prior to applying Sema3A completely abolishes Sema3A-
339 dependent death (mean: Control 2.1± 0.7; Sema3A 18.6± 3.6; Sema3A + Pep 5.9±
340 1.9) (Figure 4F-G). Thus, CBP1-4 insertion ultimately into MN axon is sufficient to block
341 CRMP4-Dyn interaction and eventually rescue Sema3A dependent MN loss
342

343 **Discussion**

344 In this work we demonstrated that Sema3A mediates MN loss via CRMP4-dynein
345 complex formation. Blocking this interaction with specific peptides rescued human
346 diseased iPSC-derived MNs from this fate (Figure 4 H). However, open questions
347 remain in this regard.
348 Our results, as well as those from other groups, suggest that Sema3A presence near
349 the axons facilitate MN axon degeneration and cell death in ALS pathology (De Winter
350 *et al.*, 2006; Körner *et al.*, 2016; Maimon and Perlson, 2019). Moreover, injecting
351 specific antibodies against NRP1 or manipulating Sema3A expression using miR126-
352 5p resulted in improvement in disease progression *in vivo* and *in vitro* (Venkova *et al.*,
353 2014; Maimon *et al.*, 2018). In contrast to these results, a recent study demonstrated
354 that crossing mice expressing a truncated form of Sema3A with $SOD1^{G93A}$ mice does
355 not result in any rescue effect (Moloney *et al.*, 2017). An explanation for this
356 contradiction could be the possibility that secreted factors such as Sema3A play a
357 more complex role in the biology of MNs (Zahavi, Maimon and Perlson, 2017). Indeed,
358 Sema3A was shown to increase the survival of MNs when added to MN cultures,
359 (Molofsky *et al.*, 2014; Birger *et al.*, 2018). Consistent with this, deletion of the Sema3A

360 gene specifically in spinal astrocytes resulted in a gradual loss of spinal MNs (Molofsky
361 *et al.*, 2014). Apparently, Sema3A may play a dual spatial role in MNs: When
362 introduced near MN axons at NMJs, it mediates their destabilization; however, when it
363 is secreted by spinal astrocytes and targets MN soma, it acts as a survival factor. Thus,
364 when targeting Sema3A for ALS, this aspect must take in consideration.
365
366 We further report that CRMP4 is elevated in ALS models. However, what mechanisms
367 are responsible for CRMP4 elevation specifically in ALS is unknown. miRNA
368 downregulation and defects in local protein synthesis are common features in several
369 ALS models (Haramati *et al.*, 2010; Costa and Willis, 2018). Along with that, Sema3A
370 was shown to induce axonal local synthesis in several neuronal systems (Campbell
371 and Holt, 2001; Wu *et al.*, 2005; Manns *et al.*, 2012; Cagnetta *et al.*, 2018, 2019). Thus,
372 we hypothesize that the elevations in CRMP4 that we observed are possibly due to
373 increase in axonal protein synthesis. Specifically, our recent published work suggest
374 that miR126-5p is downregulated in both muscles and MN axons of several ALS
375 models (Rotem *et al.*, 2017; Maimon *et al.*, 2018). Thus, it is attempting to speculate
376 further that miR126-5p downregulation mediates CRMP4 increases via local protein
377 synthesis and consolidation of retrograde death signals in ALS models. However,
378 further experiments should prove this idea.
379
380 Our data further suggest that CRMP4 forms complexes with dynein along ALS-
381 diseased MNs and leads to their loss. However, it is still not clear whether CRMP4
382 itself activates the apoptotic program or whether it plays a regulatory role by mediating
383 the arrival of the death complex. Since CRMP members were not yet reported to act
384 as transcriptional factors, we assumed that CRMP4 is indeed only one protein in a
385 bigger retrograde signaling complex. For example, JNK and c-Jun might also be part
386 of this death signal mediated by Sema3A in ALS MNs, since it was previously shown
387 that JNK signaling is elevated in ALS models and that it is a part of a retrograde death

388 signal (Perlson *et al.*, 2010; Escudero *et al.*, 2019). Another possibility is that the
389 neurotrophic receptor $p75^{NTR}$ is also involved in this process. $p75^{NTR}$ has been shown
390 to regulate a diverse range of cellular functions including axon pruning (Singh *et al.*,
391 2008) and neuronal death (Bamji *et al.*, 1998; Kenchappa *et al.*, 2010; Pathak *et al.*,
392 2018). $P75^{NTR}$ is retrogradely transported along the axon (Deinhardt *et al.*, 2006;
393 Harrington and Ginty, 2013; Cosker and Segal, 2014) and plays a role in generating a
394 retrograde apoptotic signal that activates JNK (Kenchappa *et al.*, 2010). It is
395 noteworthy that the activity of Sema3A and its receptor was recently linked to $p75^{NTR}$
396 (Ben-Zvi *et al.*, 2007). Another possible candidate that was recently shown to be
397 coupled with Sema3A is PTEN (Chadborn *et al.*, 2006). Furthermore, it was
398 established that the $p75^{NTR}$-dependent apoptosis signal is promoted by PTEN
399 activation (Song *et al.*, 2010). Thus, future experiments should examine whether
400 PTEN, $p75^{NTR}$, and JNK indeed participate in Sema3A-dependent retrograde death
401 signals in ALS.
402
403 Downregulation of CRMP4 has been previously suggested to improve
404 neurodegeneration in *in vitro* and *in vivo* ALS models (Charrier *et al.*, 2003; Duplan *et*
405 *al.*, 2010). Furthermore, *CRMP4* mutation has been associated with ALS in patients
406 (Blasco *et al.*, 2013), yet the mechanism of its action in ALS MNs has so far been
407 elusive. Here, we demonstrate a specific mechanism by which Sema3A-induced
408 CRMP4 binding to dynein is toxic in ALS. It would be interesting to determine whether
409 disease-associated *CRMP4* mutations increase the interactions of CRMP4 with
410 dynein. Indeed, the peptides we used are predicted to bind specifically at the site where
411 CRMP4 mutation occurs (Blasco *et al.*, 2013). Taken together, CRMP4 retrograde
412 death-promoting signaling may be key to MN loss in ALS.

413

414 **Methods**

415 **Animals**

416 SOD1^{G93A} (Stock No. 002726) mice were originally obtained from Jackson
417 Laboratories, and maintained by breeding with C57BL/6J mice.
418 B6;129S6-Chat$^{tm2(cre)Lowl}$/J (Stock No. 006410) and B6;129S6Gt(ROSA)26
419 Sor$^{tm14(CAG-tdTomato)Hze}$/J (Stock No. 007908) mice were originally obtained from Jackson
420 Laboratories. Animals were cross-bred in the Tel-Aviv SPF animal unit to yield
421 homozygous ChAT::Rosa^{tdTomato} mice. The ChAT::Rosa^{tdTomato} colony was maintained
422 by in-breeding males and females from the colony. The ChAT::Rosa^{tdTomato} colony was
423 cross-bred with SOD1^{G93A} to yield SOD1$^{G93A/ChAT::tdTomato}$ mice. C57BL/6 J mice were
424 used as a WT mouse strain. Mice were genotyped using the PCR reaction (KAPA Bio
425 Systems - Wilmington, MA, USA). DNA samples were generated from mouse ear or
426 tail. Animal experiments were performed under the supervision and approval of the
427 Tel-Aviv University Committee for Animal Ethics.

428

429 **IPSc Cultures**

430 Healthy/Control iPSC lines, provided by Dr. Sami Barmada, were created and
431 characterized as before (Tank *et al.*, 2018). Two lines from fALS patients carrying the
432 C9orf72 mutation, and two lines from healthy controls, were used for all experiments.

Name	**Age donated**	**Age of onset**	**Gender**	
ALS883	51	49 (Lumbar)	**M**	(>44 repeats per Athena 7/26/2012
ALS312	54	52 (Lumbar)	**M**	(44 and 2 repeats) by Athena Diagnostics 10/03/2012
Control746	58		**M**	Healthy

Control1021	54		**F**	Healthy

433

434 Colonies were groomed daily until each well of the 6-well plate was between 30% and
435 40% confluence and no spontaneously differentiated cells were observed. At this point,
436 we used the direct iMN" (diMN) differentiation in monolayers from hiPSCs protocol
437 published by Cedar Sinai and approved by Dhruv Sareen (Protocol number: CSMNC-
438 SOP-C-005) for our experiments. Briefly, we induced MN differentiation by
439 MN Differentiation Stage 1 media: prepared with – IMDM (LifeTech), F12 (LifeTech),
440 NEAA (Gibco), B27 (LifeTech), N2 (LifeTech), PSA (LifeTech), LDN193189 0.2 μM
441 (Selleck), SB431542 10 μM (Tocris), and CHIR99021 3 μM (Cayman Chemicals). The
442 media was gently added to the wells, and colonies were grown with it for 5 days. MN
443 differentiation Stage 2: At day 6 the colonies were dissociated, using accutase, and
444 100K cells were plated in the proximal compartment of our micro fluidic device. Stage
445 2 media, which contains IMDM, F12, NEAA, B27, N2, PSA, LDN193189 0.2 μM
446 (Selleck), SB431542 10 μM (Tocris), and CHIR99021 3 μM (Cayman Chemicals), All-
447 trans RA 0.1 μM (Stemgent), and SAG 1 μM (Sonic Hedgehog Agonist – Cayman
448 Chemicals) media was added to both the distal and proximal compartments of the MFC
449 and refreshed every 2 days until day 11. MN differentiation Stage 3: At day 12 the
450 media was changed to stage 3 media prepared with IMDM, F12, NEAA, B27, N2,
451 PSA, Compound E 0.1 μM (Calbiochem), DAPT 2.5 μM (Cayman Chemicals), db--
452 cAMP 0.1 μM (Millipore), Alltrans RA 0.5 μM (Stemgent), SAG 0.1 μM, Ascorbic Acid
453 200 ng/ml (Sigma), BDNF 10 ng/ml (Alomone lab), and GDNF 10 ng/ml (Alomone lab)
454 and was refreshed every 2 days until cells exhibited MN neuronal morphology and
455 positive markers. Human iPSC experiments were performed under the supervision and
456 approval of the Tel-Aviv University Committee for Human Ethics.

457

458 **Microfluidic chamber preparation**

459 Polydimethylsilxane (PDMS) microfluidic chambers (MFCs) were designed and cast
460 as described previously (Ionescu *et al.*, 2016). Briefly, MFCs were fabricated from
461 our designed templates and made from PDMS mixture at 70°C. After the wells were
462 punched, a small 'cave' was made in the explant well near the grooves using a 25G
463 needle, keeping the explant in place. Microfluidic devices were cleaned of surface
464 particles using adhesive tape and were sterilized in 70% ethanol for 15 minutes.
465 Devices were completely dried under sterile conditions using UV radiation, attached
466 to a sterile 60-mm plastic dishes (Nunc) with gentle pressure and margins were
467 sealed with PDMS before incubation at 60°C for 30 minutes to prevent the chamber
468 from detaching. Muscle channels were coated with Matrigel diluted 1:10 with DMEM
469 containing 2.5% PSN for 30 minutes at 37°C, before filling the muscle wells with
470 150μL of Bioamf-2 medium. The explant well and channel were filled with 150μL of
471 1.5 ng/mL polyornithine (P-8638, Sigma) in PBS overnight, and then replaced with
472 150 μL laminin (L-2020, Sigma), 1:333 in deionized distilled water (DDW) overnight.
473 One day before plating the spinal cord explant, laminin was replaced with explant
474 medium containing Neurobasal (Life Technologies) supplemented with 2% B27
475 (Invitrogen), 1% penicillin-streptomycin (Biological Industries), 1% Glutamax (Life
476 Technologies), 25 ng/mL brain-derived neurotrophic factor (Alomone Labs), until the
477 day on which co-culturing began.

478

479 **Motor neuron cell culture**

480 Primary spinal cord neurons were cultured using E12.5 mouse embryos of either sex
481 as previously described (Zahavi *et al.*, 2015). Briefly, spinal cords were excised,
482 trypsinized, and triturated. Supernatant was collected and centrifuged through a 4%
483 BSA cushion. The pellet was resuspended and centrifuged through an Optiprep
484 gradient (10.4% Optiprep (Sigma-Aldrich), 10 mM Tricine, 4% glucose) for 20 min at
485 760 x g with the brake turned off. Cells were collected from the interface, washed

486 once in complete medium, and then plated in coated growth chambers. Cells were
487 maintained in Complete Neurobasal Medium (Gibco) containing B27 (Gibco), 10%
488 (v/v) horse serum (Biological Industries), 25 nM beta-mercaptoethanol, 1% Penicillin-
489 Streptomycin (PS; Biological Industries), and 1% GlutaMAX (Gibco) supplemented
490 with 1 ng/mL Glial-Derived Neurotrophic Factor (GDNF), 0.5 ng/mL Ciliary
491 Neurotrophic Factor (CNTF), and 1 ng/mL Brain-Derived Neurotrophic Factor
492 (BDNF), (Alomone Labs). Prior to plating, growth plates were coated with 1.5 g/mL
493 poly D-L-ornithine (PLO; Sigma-Aldrich) overnight at 37 °C and with 3 g/mL Laminin
494 (Sigma-Aldrich) for 2 hours at 37 °C. For immunofluorescence staining, 10,000 cells
495 were plated on cover slides in 24-well plates. Cells were grown at 37 °C in 5% CO_2.
496
497 **Spinal cord explants**
498 Spinal cords were dissected from E12.5 mouse embryos of both sexes, either using
499 HB9::GFP or SOD1^{G93A} stripped of meninges and dorsal root ganglia. The ventral
500 horn was separated from the dorsal horn by longitudinal cuts along the spinal cord,
501 and transverse sections up to 1 mm were placed in the explant well**.** Prior to plating,
502 growth chambers were coated with 1.5 g/mL PLO overnight at 37 °C and 3 g/mL
503 Laminin overnight at 37 °C. Explants were maintained in Spinal Cord Explant
504 Medium containing Neurobasal, 2% B27, 1% PS, and 1% GlutaMAX, supplemented
505 with 25 ng/mL BDNF. Explants were grown at 37 °C in 5% CO_2.
506
507 **Primary myocyte culture**
508 Skeletal muscle cultures were derived from the gastrocnemius muscle of adult P60
509 female mice of either SOD1^{G93A} background or their LM using techniques previously
510 described (Ionescu *et al.*, 2016). Briefly, gastrocnemius muscles were excised and
511 incubated in 2 mg/mL collagenase I (Sigma-Aldrich) in DMEM containing 2.5%
512 penicillin-streptomycin-nystatin (PSN, Biological Industries) for 3 hours. Muscles were
513 then dissociated and incubated for 3 days in Matrigel-coated (BD Biosciences) six-

514 well plates with Bioamf-2 medium (Biological Industries) with 1% PSN at a density of
515 ~120 myofibers per well. For purification of the myoblasts, adherent cells were
516 trypsinized and pre-plated in an uncoated dish for 1 h at 37°C. Non-adherent cells
517 were then transferred into a Matrigel-coated dish with Bioamf-2 medium. Pre-plating
518 was repeated for two days, keeping the culture at less than 50% confluence, before
519 plating cells in the MFC. Cultures were maintained at 37°C and 5% CO_2. After the
520 final pre-plating, 100,000 myocytes were cultured in the pre-coated distal
521 compartment of the MFC.
522
523 **Fluorescence microscopy and image analysis**
524 All confocal images were captured using a Nikon Ti microscope equipped with a
525 Yokogawa CSU X-1 spinning disc and an Andor iXon897 EMCCD camera controlled
526 by Andor IQ3 software. All live-imaging assays were performed in a humidified
527 incubation chamber at 37°C, 5% CO_2. Images were analyzed using ImageJ software.
528
529 **Rertrograde labeling of cell bodies in the MFC**
530 Alexa Fluor 647-conjugated Cholera toxin subunit B (CTX; Thermo-Fisher C-347777)
531 at 500 ng/mL was applied to the distal compartment of an MFC system while
532 maintaining a higher liquid volume in the proximal compartment to prevent unspecific
533 labeling by diffusion. After 8 hours, only somata whose axons traversed to the distal
534 compartment were labeled.
535
536 **Recombinant Sema3A application**
537 Recombinant Sema3A (R&D,1250-S3-025) at 500 ng/mL was used in our
538 experiments. We dilute the Sema3A in poor neurobasal (PNB) containing Neurobasal
539 medium (Gibco) with 1% PS and 1% Glutamax.
540

541 **Retrograde transport inhibition**

542 In order to inhibit dynein-dependent retrograde transport, Cilliobrevin-D (Merck-
543 Millipore, 250401) at 10 μM was applied to the distal compartment of the MFC while
544 maintaining a proximal-to-distal volume gradient.

545

546 **Inhibition of dynamin-dependent endocytosis**

547 Dynasore (Sigma Aldrich, D7693) at 100nM was added to the distal compartment of
548 the MFC while maintaining a proximal-to-distal volume gradient.

549

550 **Pull down assays**.

551 For the cell cultures pull downs experiments, 2 x 10^6 COS7 cells were plated in 10 cm
552 culture dishes. The following day, cells were transfected using calcium phosphate
553 protocol with Flag-CRMP4/GFP-CRMP4/GFP-Delta-CRMP4 vector. The next day,
554 cells were lysed, and proteins were extracted using lysis buffer containing PBS, 1%
555 Triton- 100X, and 1% protease and phosphatase inhibitors (Roche), followed by
556 centrifugation and collection of the supernatant. At this point, immunoprecipitation
557 preparation of the lysate was precleared with protein-A-agarose beads (Roche).
558 Following overnight incubation with primary anti-flag antibody/anti DIC antibody,
559 complexes were incubated with protein A agarose beads for 2 h at 4 °C and then
560 precipitated and washed with PBS with 0.1% Triton X-100 (Sigma). Proteins were
561 eluted by boiling in sample buffer and then subjected to western blot precipitation
562 analysis with CRMP4/dynactin p150/Flag antibody(Sigma-Alderich F3165)/DIC. We
563 used mouse IgG antibody as a control. For sciatic nerve pull downs, 12 sciatic nerves
564 were pooled for each experiment. Here as well, the P90 sciatic nerve samples were
565 first excised and homogenized in lysis buffer containing PBS and 1% protease and
566 phosphatase inhibitors (Roche), followed by centrifugation and collection of the
567 supernatant. Then we performed the pull-down assay using the technique described

568 above. Under these conditions, pull downs were performed using DIC (Millipore
569 MAB1618) and CRMP4 (Millipore AB5454) antibodies.
570
571 **Western blotting**
572 Sciatic nerve axoplasm was isolated by excising and cutting sciatic nerves into short
573 segments, followed by detergent-free buffer homogenized with PBS X1 protease and
574 phosphatase inhibitors (Roche), followed by centrifugation and collection of the
575 supernatant. Complete sciatic nerve extracts were achieved in the same manner with
576 the exception of adding 1% Triton X-100. The protein concentration was determined
577 using the Bio-Rad Protein Assay. Protein samples were denatured by boiling in SDS
578 sample buffer and then electrophoresed in 8% polyacrylamide gels (SDS-PAGE).
579 Proteins were transferred to a nitrocellulose membrane and then immunoblotted with
580 appropriate primary antibodies: anti-CRMP4 - 1:2000 (Millipore AB5454) anti-DIC –
581 1:1000 (Millipore MAB1618) anti-p150 1:250 (BD Bioscience 611003) anti-Flag
582 1:4000 (Sigma-Alderich F3165) anti-Tubulin 1:10,000 (ab7291); and anti-tERK
583 1:10,000, diluted in 5% (w/v) Skim-milk (BD Difco) in TBS-T, followed by species-
584 specific HRP-conjugated secondary antibodies (Jackson Laboratories) and visualized
585 using a myECL imager (Thermo), according to the manufacturer's instructions.
586 ImageJ software was used for quantification.
587
588 **Sciatic nerve sectioning and immunostaining**
589 Sciatic nerves of P90 mice were isolated and immediately fixed by using 4% PFA
590 followed by 20% sucrose incubation. Then the samples were embedded by freezing
591 in Tissue-Tek® OCT. Next, 10 µm lumbar sciatic nerve sections were prepared using
592 Cryotome™ FSE cryostat (Thermo-Fisher Scientific). Sections were rinsed in PBS,
593 and then permeabilized with 0.1% Triton X-100, 5% Goat Serum (GS), 1 mg/mL
594 Bovine Serum Albumin IgG, and protease free (BSA) in PBS. Primary antibodies
595 against NFH (1:500) and CRMP4 (1:250) were diluted in blocking solution, 5% GS, 1

596 mg/mL BSA in PBS, and incubated overnight at 4°C. Samples were incubated with
597 species-specific fluorescent secondary antibodies for 2 hours at room temperature.
598 ProLong antifade medium (Molecular Probes) was added and the samples were
599 covered with a #1.5, 18×18 mm cover slide.
600
601 **Immunostaining of cell cultures**
602 Cultures were fixed in 4% paraformaldehyde and permeabilized with 0.1% Triton X-
603 100, 5% GS, 1 mg/mL BSA in PBS. Samples were blocked for 1 hour with blocking
604 medium containing 5% GS and 1 mg/mL BSA in PBS. Primary antibodies against
605 Tau 1:100 (abcam, ab80579) NFH - 1:500 (Sigma-Aldrich N4142), PlexinA1 - 1:100
606 (Alomone lab, APR-081-F), CRMP4- 1:100 (Millipore, AB5454), GAPDH 1:500
607 (abcam, ab9484), Tubulin 1:500 (abcam, ab7291), HB9 1:100 (IMGENEX, IMG-
608 6549A) were diluted in blocking solution and incubated overnight at 4°C. Samples
609 were incubated with species-specific fluorescent secondary antibodies for 2 hours at
610 room temperature. For visualizing nuclei in myotubes, DAPI was used. In the MFC,
611 after the staining protocol was completed, the MFC was peeled from the dish by
612 gently pulling it from the proximal to the distal side.
613
614 **Proximity ligation assay**
615 The proximity ligation assay (PLA) was used to visualize the co-localization of
616 selected proteins; it was performed as previously described (Söderberg *et al.*, 2008).
617 Briefly, iPSc-derived MNs and murine-MN cultures were grown in the MFC on glass
618 dishes for 18 and 5 DIV, respectively, and were then fixed in 4% PFA, at 4˚C for 20
619 minutes. Subsequently, the samples were blocked and permeabilized with 5%
620 Donkey Serum, 1% BSA, and 0.1% Triton X-100 in PBS for 1h and incubated with
621 anti-CRMP4 and anti-DIC antibodies overnight at 4˚C. Interactions (range ~40nm)
622 were detected by the proximity ligation assay Duolink kit (Sigma: PLA probe anti-
623 mouse minus DUO92004, anti-rabbit plus DUO92002, and the detection kit Far Red).

624 PLA was performed according to the manufacturer's instructions. Coverslips were
625 washed, mounted, and imaged by confocal microscopy. Half ligation samples were
626 used as a negative control. The axonal PLA signal was quantified with ImageJ
627 software using an axonal mask based on an endogenous mCherry/Rosa signal. The
628 PLA puncta signal was quantified with the analyzed particle function of the software.

629 **Peptide design and insertion into MNs**

630 The Dynein-CRMP4 blocking peptide design was based on previous findings by
631 Amrimura et al., which pointed to 50 specific amino acid sequences responsible for
632 CRMP2 binding to dynein (Arimura *et al.*, 2009). Peptides were prepared by Alomone
633 labs and GL Biochem. Peptide sequences are as follows:

634

Name	**Sequence**	**MW (Da)**
Peptide-1	TTMIIDHVVPEPE	**1480 Da**
Peptide-2	SSLTEAYEKWREWADGKS	**2143 Da**
Peptide-3	CCDYALHVDI	**1151 Da**
Peptide-4	THWNDSVKQ	**1114 Da**

635

636 The peptides were inserted into axons by harsh pipetting. The recovered axons contain
637 the peptide, as shown in Supplementary Figure 5. Tamra peptide was generously
638 donated by Dr. Mike Fainzilber's lab.

639

640 **Vectors**

641 CRMP4 and ΔCRMP4 (containing deletion of the coding sequence 301-450bp)
642 were sub-cloned in frame into the pLL3.7-GFP (Addgene) mammalian expression
643 vector. Flag-CRMP4, used in the pull-down assays, was cloned into pCDNA3 vector
644 (Invitrogen).

645

646 **Experimental design and statistical analysis**

647 All statistical analyses were performed using GraphPad Prism v6.0. For two-group
648 analysis, Student's t-test or the Mann-Whitney test was used, as determined by a
649 normality test. For multiple comparisons, Anova was used with the Tukey or Holm-
650 Sidak post-hoc tests. All experiments include at least 3 biologically independent
651 repeats, Significance was set at $p<0.05$.

652
653 **Abbreviations**
654
655 ALS - Amyotrophic Lateral Sclerosis
656 BDNF - Brain-Derived Neurotrophic Factor
657 CBP - CRMP4 Binding Peptides
658 CNTF - Ciliary Neurotrophic Factor
659 CTX – Alexa Fluor 647-conjugated Cholera toxin subunit B
660 C9orf72 - Chromosome 9 open reading frame 72
661 CRMPs – Collapsin Respond Mediator Proteins
662 DIV - Days In Vitro
663 Dyn-In - Ciliobrevin-D (Dynein Inhibitor)
664 GFP-ΔCRMP4 - CRMP4 missing amino acids 100-150
665 GDNF - Glial-Derived Neurotrophic
666 IPSC – Induced Pluripotent Stem Cells
667 JNK - c-Jun N-terminal kinases
668 MFC - Microfluidic Chambers
669 MNs - Motor Neurons
670 NMJ - Neuromuscular Junction
671 NRP1 - Neuropilin 1
672 PTEN - Phosphatase and tensin homolog
673 PLO - Poly D-L-ornithine
674 PLA - Proximity Ligation Assay
675 PDMS - Polydimethylsiloxane
676 PNB - Poor Neuorobasal medium (neurotrophin- and serum-free medium)
677 SOD1 - Cu/Zn Superoxide Dismutase 1
678 Sema3A - Semaphorin3A
679 SN – Sciatic Nervep75^{NTR} - low-affinity nerve growth factor receptor

680 **Ethics approval and consent to participate**

681 Animal experiments were performed under the supervision and approval of the Tel-
682 Aviv University Committee for Animal Ethics. Human iPSC experiments were
683 performed under the supervision and approval of the Tel-Aviv University Committee
684 for Human Ethics.

685 **Availability of data and material**

686 All data generated or analyzed during this study are included in this published article

687 **Competing interests**

688 The authors declare that they have no conflict of interest point.

689 **Funding**

690 This work was supported by the Rosetrees Trust, Alfred Taubman, the IsrALS
691 Foundation, the Israel Science Foundation (grant number 561-11), and the European
692 Research Council (grant number 309377) to E.P, Czech Health Research Council
693 grant no. NV18-04-00085 to MB, Czech Science Foundation grant no. 16-15915S to
694 MB and RW, and Grant Agency of the Charles University grants no. 524218 to RW.

695 **Author Contribution**

696 Experiment were performed by RM, LA, RW and ET. Data were collected and
697 analyzed by RM, LA. The study was designed, coordinated, and written by RM, LA,
698 RW, ET, TP, SB, MB and EP. All authors read and approved the final manuscript.

699 **Acknowledgments**

700 We thank Prof. Mike Fainzilber from the Weizmann Institute for the Tamra peptides.
701 We also thank Prof. Eva Feldman and Prof. Stephen Goutman for obtaining the
702 fibroblasts for the IPSC lines.

703 **References:**

704 Alves, C. J. *et al.* (2015) 'Gene expression profiling for human iPS-derived motor
705 neurons from sporadic ALS patients reveals a strong association between
706 mitochondrial functions and neurodegeneration', *Frontiers in Cellular Neuroscience*,

707 9, p. 289. doi: 10.3389/fncel.2015.00289.
708 Arimura, N. *et al.* (2009) 'CRMP-2 directly binds to cytoplasmic dynein and interferes
709 with its activity', *Journal of Neurochemistry*. Blackwell Publishing Ltd, 111(2), pp.
710 380–390. doi: 10.1111/j.1471-4159.2009.06317.x.
711 Balastik, M. *et al.* (2015) 'Prolyl Isomerase Pin1 Regulates Axon Guidance by
712 Stabilizing CRMP2A Selectively in Distal Axons', *Cell Reports*. Cell Press, 13(4), pp.
713 812–828. doi: 10.1016/J.CELREP.2015.09.026.
714 Bamji, S. X. *et al.* (1998) 'The p75 neurotrophin receptor mediates neuronal
715 apoptosis and is essential for naturally occurring sympathetic neuron death.', *The*
716 *Journal of cell biology*, 140(4), pp. 911–23.
717 Ben-Zvi, A. *et al.* (2007) 'Modulation of semaphorin3A activity by p75 neurotrophin
718 receptor influences peripheral axon patterning.', *The Journal of neuroscience : the*
719 *official journal of the Society for Neuroscience*, 27(47), pp. 13000–11. doi:
720 10.1523/JNEUROSCI.3373-07.2007.
721 Ben-Zvi, A. *et al.* (2008) 'The Semaphorin receptor PlexinA3 mediates neuronal
722 apoptosis during dorsal root ganglia development.', *The Journal of neuroscience : the*
723 *official journal of the Society for Neuroscience*, 28(47), pp. 12427–32. doi:
724 10.1523/JNEUROSCI.3573-08.2008.
725 Bilsland, L. G. *et al.* (2010) 'Deficits in axonal transport precede ALS symptoms in
726 vivo.', *Proceedings of the National Academy of Sciences of the United States of*
727 *America*, 107(47), pp. 20523–8. doi: 10.1073/pnas.1006869107.
728 Birger, A. *et al.* (2018) 'ALS-related human cortical and motor neurons survival is
729 differentially affected by Sema3A', *Cell Death & Disease*. Nature Publishing Group,
730 9(3), p. 256. doi: 10.1038/s41419-018-0294-6.
731 Blasco, H. *et al.* (2013) 'A Rare Motor Neuron Deleterious Missense Mutation in the
732 *DPYSL3* (*CRMP4*) Gene is Associated with ALS', *Human Mutation*. John Wiley &
733 Sons, Ltd, 34(7), pp. 953–960. doi: 10.1002/humu.22329.
734 Boillée, S., Vande Velde, C. and Cleveland, D. W. (2006) 'ALS: A Disease of Motor

735 Neurons and Their Nonneuronal Neighbors', *Neuron*, 52(1), pp. 39–59. doi:
736 10.1016/j.neuron.2006.09.018.
737 Cagnetta, R. *et al.* (2018) 'Rapid Cue-Specific Remodeling of the Nascent Axonal
738 Proteome', *Neuron*, 99(1), pp. 29-46.e4. doi: 10.1016/j.neuron.2018.06.004.
739 Cagnetta, R. *et al.* (2019) 'Noncanonical Modulation of the eIF2 Pathway Controls an
740 Increase in Local Translation during Neural Wiring', *Molecular Cell*, 73(3), pp. 474-
741 489.e5. doi: 10.1016/j.molcel.2018.11.013.
742 Campbell, D. S. and Holt, C. E. (2001) 'Chemotropic responses of retinal growth
743 cones mediated by rapid local protein synthesis and degradation.', *Neuron*, 32(6), pp.
744 1013–26.
745 Castellani, V., Falk, J. and Rougon, G. (2004) 'Semaphorin3A-induced receptor
746 endocytosis during axon guidance responses is mediated by L1 CAM.', *Molecular*
747 *and cellular neurosciences*, 26(1), pp. 89–100. doi: 10.1016/j.mcn.2004.01.010.
748 Chadborn, N. H. *et al.* (2006) 'PTEN couples Sema3A signalling to growth cone
749 collapse.', *Journal of cell science*, 119(Pt 5), pp. 951–7. doi: 10.1242/jcs.02801.
750 Charrier, E. *et al.* (2003) 'Collapsin Response Mediator Proteins (CRMPs):
751 Involvement in Nervous System Development and Adult Neurodegenerative
752 Disorders', *Molecular Neurobiology*. Humana Press, 28(1), pp. 51–64. doi:
753 10.1385/MN:28:1:51.
754 Cosker, K. E. and Segal, R. A. (2014) 'Neuronal signaling through endocytosis.', *Cold*
755 *Spring Harbor perspectives in biology*, 6(2). doi: 10.1101/cshperspect.a020669.
756 Costa, C. J. and Willis, D. E. (2018) 'To the end of the line: Axonal mRNA transport
757 and local translation in health and neurodegenerative disease', *Developmental*
758 *Neurobiology*. John Wiley & Sons, Ltd, 78(3), pp. 209–220. doi: 10.1002/dneu.22555.
759 Dang, P., Smythe, E. and Furley, A. J. W. (2012) 'TAG1 regulates the endocytic
760 trafficking and signaling of the semaphorin3A receptor complex.', *The Journal of*
761 *neuroscience : the official journal of the Society for Neuroscience*, 32(30), pp. 10370–
762 82. doi: 10.1523/JNEUROSCI.5874-11.2012.

763 Deinhardt, K. *et al.* (2006) 'Rab5 and Rab7 Control Endocytic Sorting along the
764 Axonal Retrograde Transport Pathway', *Neuron*, 52(2), pp. 293–305. doi:
765 10.1016/j.neuron.2006.08.018.
766 DeJesus-Hernandez, M. *et al.* (2011) 'Expanded GGGGCC Hexanucleotide Repeat
767 in Noncoding Region of C9ORF72 Causes Chromosome 9p-Linked FTD and ALS',
768 *Neuron*. Elsevier, 72(2), pp. 245–256. doi: 10.1016/J.NEURON.2011.09.011.
769 Devlin, A.-C. *et al.* (2015) 'Human iPSC-derived motoneurons harbouring TARDBP
770 or C9ORF72 ALS mutations are dysfunctional despite maintaining viability', *Nature*
771 *Communications*. Nature Publishing Group, 6(1), p. 5999. doi:
772 10.1038/ncomms6999.
773 Duplan, L. *et al.* (2010) 'Collapsin response mediator protein 4a (CRMP4a) is
774 upregulated in motoneurons of mutant SOD1 mice and can trigger motoneuron
775 axonal degeneration and cell death.', *The Journal of neuroscience : the official journal*
776 *of the Society for Neuroscience*, 30(2), pp. 785–96. doi: 10.1523/JNEUROSCI.5411-
777 09.2010.
778 Escudero, C. A. *et al.* (2019) 'c-Jun N-terminal kinase (JNK)-dependent
779 internalization and Rab5-dependent endocytic sorting mediate long-distance
780 retrograde neuronal death induced by axonal BDNF-p75 signaling', *Scientific*
781 *Reports*. Nature Publishing Group, 9(1), p. 6070. doi: 10.1038/s41598-019-42420-6.
782 Fischer, L. R. *et al.* (2004) 'Amyotrophic lateral sclerosis is a distal axonopathy:
783 evidence in mice and man.', *Experimental neurology*, 185(2), pp. 232–40.
784 Fournier, A. E. *et al.* (2000) 'Semaphorin3a Enhances Endocytosis at Sites of
785 Receptor–F-Actin Colocalization during Growth Cone Collapse', *The Journal of Cell*
786 *Biology*, 149(2), pp. 411–422. doi: 10.1083/jcb.149.2.411.
787 Frey, D. *et al.* (2000) 'Early and selective loss of neuromuscular synapse subtypes
788 with low sprouting competence in motoneuron diseases.', *The Journal of*
789 *neuroscience : the official journal of the Society for Neuroscience*, 20(7), pp. 2534–
790 42.

791 Fujimori, K. *et al.* (2018) 'Modeling sporadic ALS in iPSC-derived motor neurons
792 identifies a potential therapeutic agent', *Nature Medicine*. Nature Publishing Group,
793 24(10), pp. 1579–1589. doi: 10.1038/s41591-018-0140-5.
794 Gershoni-Emek, N. *et al.* (2015) 'Amyotrophic Lateral Sclerosis as a Spatiotemporal
795 Mislocalization Disease: Location, Location, Location', *International Review of Cell*
796 *and Molecular Biology*. Academic Press, 315, pp. 23–71. doi:
797 10.1016/BS.IRCMB.2014.11.003.
798 Gibbs, K. L. *et al.* (2018) 'Inhibiting p38 MAPK alpha rescues axonal retrograde
799 transport defects in a mouse model of ALS', *Cell Death & Disease*. Nature Publishing
800 Group, 9(6), p. 596. doi: 10.1038/s41419-018-0624-8.
801 Good, P. F. *et al.* (2004) 'A role for semaphorin 3A signaling in the degeneration of
802 hippocampal neurons during Alzheimer's disease.', *Journal of neurochemistry*, 91(3),
803 pp. 716–36. doi: 10.1111/j.1471-4159.2004.02766.x.
804 Goshima, Y. *et al.* (1997) 'A novel action of collapsin: collapsin-1 increases antero-
805 and retrograde axoplasmic transport independently of growth cone collapse.', *Journal*
806 *of neurobiology*, 33(3), pp. 316–28.
807 Haramati, S. *et al.* (2010) 'miRNA malfunction causes spinal motor neuron disease.',
808 *Proceedings of the National Academy of Sciences of the United States of America*,
809 107(29), pp. 13111–6. doi: 10.1073/pnas.1006151107.
810 Harrington, A. W. and Ginty, D. D. (2013) 'Long-distance retrograde neurotrophic
811 factor signalling in neurons.', *Nature reviews. Neuroscience*. Nature Publishing
812 Group, a division of Macmillan Publishers Limited. All Rights Reserved., 14(3), pp.
813 177–87. doi: 10.1038/nrn3253.
814 Howard, J., Hudspeth, A. J. and Vale, R. D. (1989) 'Movement of microtubules by
815 single kinesin molecules', *Nature*. Nature Publishing Group, 342(6246), pp. 154–158.
816 doi: 10.1038/342154a0.
817 Ibáñez, C. F. (2007) 'Message in a bottle: long-range retrograde signaling in the
818 nervous system', *Trends in Cell Biology*. Elsevier Current Trends, 17(11), pp. 519–

819 528. doi: 10.1016/J.TCB.2007.09.003.
820 Ionescu, A. *et al.* (2016) 'Compartmental microfluidic system for studying muscle–
821 neuron communication and neuromuscular junction maintenance', *European Journal*
822 *of Cell Biology*, 95(2), pp. 69–88. doi: 10.1016/j.ejcb.2015.11.004.
823 Ionescu, A. *et al.* (2019) 'Targeting the Sigma-1 Receptor via Pridopidine Ameliorates
824 Central Features of ALS Pathology in a SOD1G93A Model', *Cell Death & Disease*.
825 Nature Publishing Group, 10(3), p. 210. doi: 10.1038/s41419-019-1451-2.
826 Kenchappa, R. S. *et al.* (2010) 'p75 neurotrophin receptor-mediated apoptosis in
827 sympathetic neurons involves a biphasic activation of JNK and up-regulation of tumor
828 necrosis factor-alpha-converting enzyme/ADAM17.', *The Journal of biological*
829 *chemistry*, 285(26), pp. 20358–68. doi: 10.1074/jbc.M109.082834.
830 Körner, S. *et al.* (2016) 'The Axon Guidance Protein Semaphorin 3A Is Increased in
831 the Motor Cortex of Patients With Amyotrophic Lateral Sclerosis.', *Journal of*
832 *neuropathology and experimental neurology*. The Oxford University Press, p. nlw003.
833 doi: 10.1093/jnen/nlw003.
834 LaMonte, B. H. *et al.* (2002) 'Disruption of dynein/dynactin inhibits axonal transport in
835 motor neurons causing late-onset progressive degeneration.', *Neuron*, 34(5), pp.
836 715–27.
837 Lee, S. and Huang, E. J. (2017) 'Modeling ALS and FTD with iPSC-derived neurons',
838 *Brain Research*. Elsevier, 1656, pp. 88–97. doi: 10.1016/J.BRAINRES.2015.10.003.
839 Luo, Y., Raible, D. and Raper, J. A. (1993) 'Collapsin: a protein in brain that induces
840 the collapse and paralysis of neuronal growth cones.', *Cell*, 75(2), pp. 217–27.
841 Maimon, R. *et al.* (2018) 'miR126-5p Downregulation Facilitates Axon Degeneration
842 and NMJ Disruption via a Non-Cell-Autonomous Mechanism in ALS.', *The Journal of*
843 *neuroscience : the official journal of the Society for Neuroscience*. Society for
844 Neuroscience, 38(24), pp. 5478–5494. doi: 10.1523/JNEUROSCI.3037-17.2018.
845 Maimon, R. and Perlson, E. (2019) 'Muscle secretion of toxic factors, regulated by
846 miR126-5p, facilitates motor neuron degeneration in amyotrophic lateral sclerosis',

847 *Neural Regeneration Research*, 14(6), p. 969. doi: 10.4103/1673-5374.250571.
848 Manns, R. P. C. *et al.* (2012) 'Differing semaphorin 3A concentrations trigger distinct
849 signaling mechanisms in growth cone collapse.', *The Journal of neuroscience : the*
850 *official journal of the Society for Neuroscience*. Europe PMC Funders, 32(25), pp.
851 8554–9. doi: 10.1523/JNEUROSCI.5964-11.2012.
852 Millecamps, S. and Julien, J.-P. (2013) 'Axonal transport deficits and
853 neurodegenerative diseases', *Nature Reviews Neuroscience*. Nature Publishing
854 Group, 14(3), pp. 161–176. doi: 10.1038/nrn3380.
855 Molofsky, A. V *et al.* (2014) 'Astrocyte-encoded positional cues maintain
856 sensorimotor circuit integrity.', *Nature*, 509(7499), pp. 189–94. doi:
857 10.1038/nature13161.
858 Moloney, E. B. *et al.* (2017) 'Expression of a Mutant SEMA3A Protein with
859 Diminished Signalling Capacity Does Not Alter ALS-Related Motor Decline, or Confer
860 Changes in NMJ Plasticity after BotoxA-Induced Paralysis of Male Gastrocnemic
861 Muscle', *PLOS ONE*. Edited by B. Key. Public Library of Science, 12(1), p.
862 e0170314. doi: 10.1371/journal.pone.0170314.
863 Moloney, E. B., de Winter, F. and Verhaagen, J. (2014) 'ALS as a distal axonopathy:
864 molecular mechanisms affecting neuromuscular junction stability in the
865 presymptomatic stages of the disease.', *Frontiers in neuroscience*, 8, p. 252. doi:
866 10.3389/fnins.2014.00252.
867 Münch, C. *et al.* (2004) 'Point mutations of the p150 subunit of dynactin (DCTN1)
868 gene in ALS.', *Neurology*. Wolters Kluwer Health, Inc. on behalf of the American
869 Academy of Neurology, 63(4), pp. 724–6. doi:
870 10.1212/01.wnl.0000134608.83927.b1.
871 Nagai, J. *et al.* (2015) 'Crmp4 deletion promotes recovery from spinal cord injury by
872 neuroprotection and limited scar formation', *Scientific Reports*. Nature Publishing
873 Group, 5(1), p. 8269. doi: 10.1038/srep08269.
874 Nagai, J., Baba, R. and Ohshima, T. (2017) 'CRMPs Function in Neurons and Glial

875 Cells: Potential Therapeutic Targets for Neurodegenerative Diseases and CNS
876 Injury', *Molecular Neurobiology*, 54(6), pp. 4243–4256. doi: 10.1007/s12035-016-
877 0005-1.
878 Nakamura, F., Kalb, R. G. and Strittmatter, S. M. (2000) 'Molecular basis of
879 semaphorin-mediated axon guidance.', *Journal of neurobiology*, 44(2), pp. 219–29.
880 Nicolas, A. *et al.* (2018) 'Genome-wide Analyses Identify KIF5A as a Novel ALS
881 Gene', *Neuron*. Cell Press, 97(6), pp. 1268-1283.e6. doi:
882 10.1016/J.NEURON.2018.02.027.
883 Olenick, M. A., Dominguez, R. and Holzbaur, E. L. F. (2019) 'Dynein activator Hook1
884 is required for trafficking of BDNF-signaling endosomes in neurons', *The Journal of*
885 *Cell Biology*, 218(1), pp. 220–233. doi: 10.1083/jcb.201805016.
886 Paschal, B. M. and Vallee, R. B. (1987) 'Retrograde transport by the microtubule-
887 associated protein MAP 1C', *Nature*. Nature Publishing Group, 330(6144), pp. 181–
888 183. doi: 10.1038/330181a0.
889 Pathak, A. *et al.* (2018) 'Retrograde Degenerative Signaling Mediated by the p75
890 Neurotrophin Receptor Requires p150Glued Deacetylation by Axonal HDAC1',
891 *Developmental Cell*. Cell Press, 46(3), pp. 376-387.e7. doi:
892 10.1016/J.DEVCEL.2018.07.001.
893 Perlson, E. *et al.* (2009) 'A switch in retrograde signaling from survival to stress in
894 rapid-onset neurodegeneration.', *The Journal of neuroscience : the official journal of*
895 *the Society for Neuroscience*, 29(31), pp. 9903–17. doi: 10.1523/JNEUROSCI.0813-
896 09.2009.
897 Perlson, E. *et al.* (2010) 'Retrograde axonal transport: pathways to cell death?',
898 *Trends in neurosciences*, 33(7), pp. 335–44. doi: 10.1016/j.tins.2010.03.006.
899 Peters, O. M., Ghasemi, M. and Brown, R. H. (2015) 'Emerging mechanisms of
900 molecular pathology in ALS.', *The Journal of clinical investigation*, 125(5), pp. 1767–
901 79. doi: 10.1172/JCI71601.
902 Ponnusamy, R. *et al.* (2014) 'Crystal Structure of Human Crmp-4: Correction of

903 Intensities for Lattice-Translocation Disorder', *Acta Crystallogr.,Sect.D*, 70, p. 1680.
904 doi: 10.2210/PDB4CNT/PDB.
905 Rahajeng, J. *et al.* (2010) 'Collapsin Response Mediator Protein-2 (Crmp2)
906 Regulates Trafficking by Linking Endocytic Regulatory Proteins to Dynein Motors',
907 *Journal of Biological Chemistry*, 285(42), pp. 31918–31922. doi:
908 10.1074/jbc.C110.166066.
909 Renton, A. E. *et al.* (2011) 'A Hexanucleotide Repeat Expansion in C9ORF72 Is the
910 Cause of Chromosome 9p21-Linked ALS-FTD', *Neuron*, 72(2), pp. 257–268. doi:
911 10.1016/j.neuron.2011.09.010.
912 Rosen, D. R. *et al.* (1993) 'Mutations in Cu/Zn superoxide dismutase gene are
913 associated with familial amyotrophic lateral sclerosis', *Nature*, 362(6415), pp. 59–62.
914 doi: 10.1038/362059a0.
915 Rotem, N. *et al.* (2017) 'ALS Along the Axons – Expression of Coding and Noncoding
916 RNA Differs in Axons of ALS models', *Scientific Reports*. Nature Publishing Group, 7,
917 p. 44500. doi: 10.1038/srep44500.
918 Sances, S. *et al.* (2016) 'Modeling ALS with motor neurons derived from human
919 induced pluripotent stem cells', *Nature Neuroscience*. Nature Publishing Group,
920 19(4), pp. 542–553. doi: 10.1038/nn.4273.
921 Sasaki, Y. *et al.* (2002) 'Fyn and Cdk5 Mediate Semaphorin-3A Signaling, Which Is
922 Involved in Regulation of Dendrite Orientation in Cerebral Cortex', *Neuron*. Cell
923 Press, 35(5), pp. 907–920. doi: 10.1016/S0896-6273(02)00857-7.
924 Schmidt, E. F. and Strittmatter, S. M. (2007) 'The CRMP Family of Proteins and Their
925 Role in Sema3A Signaling', in *Semaphorins: Receptor and Intracellular Signaling*
926 *Mechanisms*. New York, NY: Springer New York, pp. 1–11. doi: 10.1007/978-0-387-
927 70956-7_1.
928 Shi, Y. *et al.* (2018) 'Haploinsufficiency leads to neurodegeneration in C9ORF72
929 ALS/FTD human induced motor neurons', *Nature Medicine*. Nature Publishing
930 Group, 24(3), pp. 313–325. doi: 10.1038/nm.4490.

931 Singh, K. K. *et al.* (2008) 'Developmental axon pruning mediated by BDNF-p75NTR-
932 dependent axon degeneration.', *Nature neuroscience*, 11(6), pp. 649–58. doi:
933 10.1038/nn.2114.
934 Söderberg, O. *et al.* (2008) 'Characterizing proteins and their interactions in cells and
935 tissues using the in situ proximity ligation assay', *Methods*. Academic Press, 45(3),
936 pp. 227–232. doi: 10.1016/J.YMETH.2008.06.014.
937 Song, W. *et al.* (2010) 'ProNGF induces PTEN via p75NTR to suppress Trk-mediated
938 survival signaling in brain neurons.', *The Journal of neuroscience : the official journal*
939 *of the Society for Neuroscience*, 30(46), pp. 15608–15. doi:
940 10.1523/JNEUROSCI.2581-10.2010.
941 Steinberg, K. M. *et al.* (2015) 'Exome sequencing of case-unaffected-parents trios
942 reveals recessive and de novo genetic variants in sporadic ALS', *Scientific Reports*.
943 Nature Publishing Group, 5(1), p. 9124. doi: 10.1038/srep09124.
944 Tank, E. M. *et al.* (2018) 'Abnormal RNA stability in amyotrophic lateral sclerosis',
945 *Nature Communications*. Nature Publishing Group, 9(1), p. 2845. doi:
946 10.1038/s41467-018-05049-z.
947 Terenzio, M., Schiavo, G. and Fainzilber, M. (2017) 'Compartmentalized Signaling in
948 Neurons: From Cell Biology to Neuroscience', *Neuron*. Cell Press, 96(3), pp. 667–
949 679. doi: 10.1016/J.NEURON.2017.10.015.
950 Valdez, G. *et al.* (2012) 'Shared resistance to aging and ALS in neuromuscular
951 junctions of specific muscles.', *PloS one*. Public Library of Science, 7(4), p. e34640.
952 doi: 10.1371/journal.pone.0034640.
953 Venkova, K. *et al.* (2014) 'Semaphorin 3A signaling through neuropilin-1 is an early
954 trigger for distal axonopathy in the SOD1G93A mouse model of amyotrophic lateral
955 sclerosis.', *Journal of neuropathology and experimental neurology*. The Oxford
956 University Press, 73(7), pp. 702–13. doi: 10.1097/NEN.0000000000000086.
957 De Vos, K. J. and Hafezparast, M. (2017) 'Neurobiology of axonal transport defects
958 in motor neuron diseases: Opportunities for translational research?', *Neurobiology of*

959 *Disease*. Academic Press, 105, pp. 283–299. doi: 10.1016/J.NBD.2017.02.004.
960 Wehner, A. B. *et al.* (2016) 'Semaphorin 3A is a retrograde cell death signal in
961 developing sympathetic neurons.', *Development (Cambridge, England)*, 143(9), pp.
962 1560–70. doi: 10.1242/dev.134627.
963 Wen, X. *et al.* (2014) 'Antisense Proline-Arginine RAN Dipeptides Linked to
964 C9ORF72-ALS/FTD Form Toxic Nuclear Aggregates that Initiate In Vitro and In Vivo
965 Neuronal Death', *Neuron*, 84(6), pp. 1213–1225. doi: 10.1016/j.neuron.2014.12.010.
966 De Winter, F. *et al.* (2006) 'The expression of the chemorepellent Semaphorin 3A is
967 selectively induced in terminal Schwann cells of a subset of neuromuscular synapses
968 that display limited anatomical plasticity and enhanced vulnerability in motor neuron
969 disease.', *Molecular and cellular neurosciences*, 32(1–2), pp. 102–17. doi:
970 10.1016/j.mcn.2006.03.002.
971 de Wit, J. *et al.* (2006) 'Vesicular trafficking of semaphorin 3A is activity-dependent
972 and differs between axons and dendrites.', *Traffic (Copenhagen, Denmark)*, 7(8), pp.
973 1060–77. doi: 10.1111/j.1600-0854.2006.00442.x.
974 Wu, K. Y. *et al.* (2005) 'Local translation of RhoA regulates growth cone collapse.',
975 *Nature*. NIH Public Access, 436(7053), pp. 1020–1024. doi: 10.1038/nature03885.
976 Yamashita, N. *et al.* (2014) 'Plexin-A4-dependent retrograde semaphorin 3A
977 signalling regulates the dendritic localization of GluA2-containing AMPA receptors.',
978 *Nature communications*, 5, p. 3424. doi: 10.1038/ncomms4424.
979 Yamashita, N. and Goshima, Y. (2012) 'Collapsin Response Mediator Proteins
980 Regulate Neuronal Development and Plasticity by Switching Their Phosphorylation
981 Status', *Molecular Neurobiology*, 45(2), pp. 234–246. doi: 10.1007/s12035-012-8242-
982 4.
983 Zahavi, E. E. *et al.* (2015) 'A compartmentalized microfluidic neuromuscular co-
984 culture system reveals spatial aspects of GDNF functions.', *Journal of cell science*,
985 128(6), pp. 1241–52. doi: 10.1242/jcs.167544.
986 Zahavi, E. E., Maimon, R. and Perlson, E. (2017) 'Spatial-specific functions in

987 retrograde neuronal signalling', *Traffic*. John Wiley & Sons A/S. doi:
988 10.1111/tra.12487.
989
990
991 **Figure Legends**
992 **Figure 1 – Sema3A activates a retrograde death signal in ALS mutated motor**
993 **neurons.**
994 (A) Simplified illustration of the compartmentalized MFC used to culture $WT^{ChAT::tdTomato}$
995 / $SOD1^{G93A/ChAT::tdTomato}$ spinal cord explants together with WT/ $SOD1^{G93A}$ primary
996 myocytes in two different compartments. (B) Representative images of either
997 $SOD1^{G93A/ChAT::tdTomato}$ or $WT^{ChAT::tdTomato}$ spinal cord explants in the proximal
998 compartment of MFCs in four different co-culture combinations at 10DIV and at 15DIV.
999 Images display significant motor neuron loss in $SOD1^{G93A/ChAT::tdTomato}$ explant-cultured
1000 $SOD1^{G93A}$ myocytes. Scale bar: 20 µm. (C) Quantification of the percentage of
1001 surviving cells per explant at 15DIV in co-culture compared to 10DIV (n = 3, One-way
1002 ANOVA, Tukey's multiple comparisons test ; p =0.0013, p=0.0001, p=0.036 ; WT-WT
1003 vs $SOD1^{G93A}$- $SOD1^{G93A}$, WT-WT vs WT- $SOD1^{G93A}$, $SOD1^{G93A}$- $SOD1^{G93A}$ vs WT-
1004 $SOD1^{G93A}$). (D) Left panel - Illustration of the experimental procedure for MNs in an
1005 MFC treated with the fluorescently tagged retrograde tracer CTX in the distal
1006 compartment. Neuronal cell bodies in the explant whose axons have traversed into the
1007 distal compartment were also labeled by the retrograde tracer. Right Panel -
1008 Representative images show CTX^+ axons in the distal compartment and their cell
1009 bodies in the proximal compartment after applying Sema3A to the distal compartment.
1010 Gray denotes CTX tagging. Scale bar: 20µm. (E) Quantification of the CTX^+ cell bodies
1011 in a WT explant 2 days after applying Sema3A to the distal compartment revealed no
1012 change in the cell count compared with the control. (F) Quantification of CTX^+ in a
1013 $SOD1^{G93A}$ explant 2 days after applying Sema3A to the distal compartment revealed a
1014 decreased number of CTX^+ cell bodies, which can be blocked by a parallel application

1015 of the dynein inhibitor Cilliobrevin-D (Dyn-In) with Sema3A; however, a parallel
1016 application of Dynasore with Sema3A did not have a similar effect. Quantification is
1017 the percentage of total CTX^+ cells after applying Sema3A compared to control medium;
1018 plots show mean ±SEM, (One-way ANOVA, Tukey's multiple comparisons test, n = 3;
1019 *p<0.05, **p<0.01) dynein inhibitor and Dynasore treatments were used as a negative
1020 control. (G) Representative images of WT and C9orf72 Human IPSc-derived MNs
1021 before and after applying Sema3A, tagged with CTX using the same described
1022 technique. Green denotes CTX-positive cells. Scale bar: 100 µm. (H-I) Quantification
1023 of CTX^+ in WT IPSc-derived MNs revealed no change in cell count 3 days after
1024 applying Sema3A distal compared with the control. However, applying Sema3A to the
1025 distal compartment of *C9orf72* iPSC-derived MNs resulted in a significant loss after 3
1026 days. Quantification is the percentage of total CTX^+ cells after applying Sema3A
1027 compared to control medium and is shown as the mean ±SEM (Student's t-test, n=3,
1028 *p<0.05)
1029
1030 **Figure 2 – CRMP4 elevation in ALS models**
1031 (A-B) Western blot analysis and quantification of P90 SN tissues revealed that the
1032 levels of CRMP4 are elevated in *SOD1*^{G93A} SN compared with their corresponding WT
1033 control. tERK was used as a loading control (Student's t-test, n = 3, *p = 0.0215). (C)
1034 Representative images of fixed and immunostained SN cross sections showing
1035 elevation in the co-localization area of CRMP4 and NFH in the SOD1^{G93A} group
1036 compared with its WT. Red denotes NFH, Green denotes CRMP4. Left panel scale
1037 bar: 10 µm. Right panel is an inset - Scale bar: 5 µm. (D) Quantification of the images
1038 in C revealed a significant difference between the WT and *SOD1*^{G93} conditions
1039 (Student's t-test, n = 3, *p = 0.042). (E) Representative images of fixed and stained
1040 healthy or *C9orf72* iPSC-derived MNs treated with Sema3A or control in the distal
1041 compartment for 6 h. Red denotes Tubulin, Green denotes CRMP4. Scale bar: 5 µm.
1042 (F) Quantification of the images in E reveals a significant increase in the *C9orf72* iPSC-

1043 derived MN group treated with Sema3A. (One-way ANOVA, Tukey's multiple
1044 comparisons test, n = 3, *p = 0.042.)
1045
1046 **Figure 3 - CRMP4 and dynein complex formation in ALS models.**
1047 (A) Immunoprecipitation of DIC followed by western blot analysis of CRMP4 showing
1048 a strong association of DIC with CRMP4 in SOD1^{G93A} SNs compared to WT SNs under
1049 physiological conditions. IgG antibody was used as a control. (B) Quantification of 3
1050 pull down repeats with anti-DIC revealed a significantly stronger interaction of DIC with
1051 CRMP4 in *SOD1^{G93A}* compared with its WT. The CRMP4 intensity band was
1052 normalized to the DIC intensity band in each repeat. (Ratio Paired t-test, n = 3, 12 SN
1053 were used in each repeat, *p = 0.0416). (C) Illustration of the experimental procedure
1054 for the proximity ligation assay in an MFC. (D) Representative images of the Proximity
1055 ligation assay using CRMP4 and dynein antibodies in healthy and diseased mouse
1056 MNs that were exposed to either control or the Sema3A 8 h prior to fixation. (E)
1057 Quantification of the images in D revealed an increase in the CRMP4-DIC puncta
1058 number per axon in the Sema3A-treated group. CRMP4-DIC puncta number per axon
1059 was further increase when counting Sema3A-treated MNs carrying the *SOD1^{G93A}*
1060 mutation (Student's t-test, n = 3). (F) Representative images of the CRMP4-DIC
1061 puncta number per axon in human iPSC-derived MNs. (G) Bar graph shows an
1062 increase in the CRMP4-DIC puncta number in *C9orf72* iPSC- derived MNs that were
1063 treated with Sema3A compared with their healthy control (Mann Whitney test, n = 3,
1064 ***p = 0.0003). (H) Illustration of the experimental procedure for iPSC-derived MNs in
1065 an MFC treated with the fluorescently tagged retrograde tracer CTX in the distal
1066 compartment. Neuronal cell bodies whose axons have traversed into the distal
1067 compartment were marked by the retrograde tracer. Then, the distal axons were
1068 treated with Sema3A or control and the intensity of CRMP4 was measured either in
1069 the cell body or in the proximal axons. (I) Representative images (left panel) of proximal
1070 axons that were fixed and stained for CRMP4 and GAPDH after Sema3A/Sema3A

1071 dynein inhibitor or control treatment. Green denotes CRMP4, Red denotes GAPDH.
1072 Scale bar: 5um. (Right panel) Quantification of the images' intensity revealed an
1073 increase in CRMP4 expression after Sema3A treatment compared with control
1074 treatment. This effect was diminished when dynein inhibitor was applied prior to
1075 Sema3A treatment, suggesting an increase in CRMP4 intensity due to retrograde
1076 movement. (J) Representative images (left panel) of cell somata that were fixed and
1077 stained for CRMP4 and GAPDH after Sema3A/Sema3A dynein inhibitor or control
1078 treatment. Gray denotes CTX, Green denotes CRMP4, Red denotes GAPDH. Scale
1079 bar: 5um. (Right panel) Quantification of the images' intensity revealed an increase in
1080 CRMP4 expression after Sema3A treatment compared with control treatment that was
1081 reduced after dynein inhibitor application, (n = 3, One-way ANOVA, Tukey's multiple
1082 comparisons test; *p =0.013, *p=0.0001). (K) Quantification of the cell somata area
1083 under the same conditions as in J shows that Sema3A treatment in the distal axons
1084 results in a decreased cell area. However, this effect was diminished when dynein
1085 inhibitors were applied prior to Sema3A treatment (n = 3, One-way ANOVA, Tukey's
1086 multiple comparisons test; **p =0.0067, **p=0.0031).
1087
1088 **Figure 4 - Specific peptides interfere with CRMP4-dynein interaction and rescue**
1089 **MN cell death**
1090 (A) Crystal structure (PDB code 4CNT) of CRMP4 monomer (upper panel) and
1091 biological tetramer assembly (lower panel). The derived peptides that were selected
1092 are highlited and color coded as indicated. Note that the peptides' sequences are
1093 located on the surface of the protein away from the intermolecular tetramization
1094 interfaces. (B) Upper panel - immunoprecipitation of DIC followed by western blot
1095 analysis of CRMP4 showing a strong association of dynein complex with CRMP4 in
1096 COS7 cells overexpressing GFP-CRMP4. This binding completely abolished after
1097 deletion of amino acid 100-150 and can be interrupted with by pre-incubation of the
1098 protein extract with a 10 um mixture of CBP1-4. Lower panel - Total protein western

1099 blot analysis indicates similar protein levels before the pull-down assay. (C)
1100 Quantification of the blot in B shows a significant decrease in CRMP4-dynactin binding
1101 with GFP-ΔCRMP4 and with CBP1-4 pre-incubation, compared with control. The
1102 dynactin intensity band normalized to the Flag-CRMP4 intensity band in each repeat
1103 (One-way ANOVA, Tukey's multiple comparisons test **p=0.007,*p=0.02, n=3). (D-E)
1104 Representative images and quantification of the proximity ligation assay for CRMP4-
1105 dynein with and without peptides reveal a decrease in the puncta number in C9orf72
1106 iPSC-derived MNs after peptide application (Student's t-test, p=0.0001, n=3). (F-G)
1107 Representative images and quantification of C9orf72 iPSC-derived MNs in the
1108 proximal compartment of an MFC before and after Sema3A treatment with and without
1109 10 ug CBP1-4. The data indicate a significant 25% MN loss after applying Sema3A,
1110 which was prevented when Sema3A and the peptide mixture were introduced together.
1111 Green denotes CTX-positive cells. Scale bar: 100 um (n = 3, One-way ANOVA,
1112 Tukey's multiple comparisons test; **p =0.004, **p=0.004). (H) Model - Sema3A
1113 mediates MN loss via CRMP4-Dynein complex formation. Blocking this interaction with
1114 specific peptides rescues human diseased iPSC-derived MNs from this fate.
1115
1116 **Supplementary Figure 1: Dynasore blocks internalization of the Sema3A binding**
1117 **receptor**
1118 (A) Representative images of COS7 cells that were grown on glass dishes for 2DIV
1119 and then treated with FITC-PlexinA1 antibody with and without Dynasore. The Plexin
1120 A1-FITC antibody remained on the cell surface of cells that were treated with the
1121 dynamin-dependent endocytosis blocker compared with the untreated group.
1122
1123 **Supplementary Figure 2: Human iPSC-derived motor neurons in a Microfluidic**
1124 **Device.**
1125 (A) Representative image of C9orf72 mCherry-tagged iPSC colonies grown on
1126 Matrigel coating and treated with Nutristem media. The colonies were grown until they

1127 reach the right size for MN differentiation protocol. (B) Left panel - Representative
1128 image of differentiated C9orf72 mCherry-tagged iPSC colonies grown on laminin in our
1129 MFC treated with stage 2 differentiation media containing IMDM, F12, NEAA, B27,
1130 N2,PSA, LDN193189, SB431542, CHIR99021, All-Trans RA, and *SAG for another 6
1131 DIV. Neuron-like morphology was achieved. Then the cells were treated with stage 3
1132 media containing IMDM, F12, NEAA, B27, N2, PSA, Compound E, DAPT, db-cAMP,
1133 All-Trans RA, *SAG, and Ascorbic Acid until adult MN morphology and function were
1134 achieved (right panel). (C) Stage 3 iPSC-derived MNs reach out their axons into the
1135 microgrooves toward the proximal compartment after 18 DIV. (D) iPSC-derived MNs
1136 were fixed and stained at 18 DIV in the proximal compartment of the MFC for motor
1137 neuron specific markers. Green denotes tubulin, Blue denotes DAPI, and Red denotes
1138 HB9. Scale bar. (E) iPSC-derived MNs were fixed and stained at 18DIV in the distal
1139 compartment of the MFC for NFH and Tubulin. Scale bar. (F) Representative images
1140 for both proximal and distal compartments showing Tau-positive staining of our iPSC-
1141 derived MN cultures in both compartments.
1142
1143 **Supplementary Figure 3: Peptide insertion into COS7 and MNs**
1144 (A) Upper panel - immunoprecipitation assay with anti-flag antibody followed by
1145 western blot analysis of dynactin (p150) showing a strong association of dynein
1146 complex with CRMP4 in COS7 overexpressing Flaf-CRMP4 protein. This binding can
1147 be interrupted with pre-incubation of the protein extract with a 10μm mixture of CBP1-
1148 4. Lower panel - Total protein western blot analysis indicates similar protein levels
1149 before the pull-down assay. (B) Quantification of the blot in A shows a significant
1150 decrease in Flag-CRMP4-dynactin binding when peptides were pre-incubated with the
1151 cell lysate compared with control. The dynactin intensity band normalized to the Flag-
1152 CRMP4 intensity band in each repeat (Student's t-test, p=0.01, n=3). (C) Upper panel
1153 - Immunoprecipitation assay with anti-flag antibody followed by western blot analysis

1154 of dynactin (p150) showing a strong association of dynein complex with CRMP4 in
1155 COS7 overexpressing Flag-CRMP4 protein. This binding was tested by pre-incubation
1156 of the protein extract with 10µm of CBP1-4. Lower panel - Total protein western blot
1157 analysis indicates similar protein levels before the pull-down assay. (D) Quantification
1158 of the blot in C shows a mild but significant decrease in Flag-CRMP4-dynactin binding
1159 only when CBP4 was used, suggesting minimal effects on CRMP4-dynein complex
1160 binding for CBP1-3 in isolation. The dynactin intensity band normalized to the Flag-
1161 CRMP4 intensity band in each repeat (Student's t-test, p=0.05, n=3).
1162 E) Representative images of MN culture after insertion of TAMRA peptides by harsh
1163 pipetting. The cells were stained with DAPI (Blue) and Calcein (Green). Red denotes
1164 TAMRA peptide. Scale bar: 100um. (F) Higher magnification images of MN axons in
1165 the distal compartment of an MFC after treatment with TAMRA peptide specifically in
1166 the axon compartment. Scale bar: 5um.
1167 **Movie 1 – Dynein-dependent retrograde transport of Lysotracker and Mitotracker**
1168 **in MN axons.**
1169 Time-lapse image series of lysosomal (green) and mitochondrial (red) trackers
1170 undergo dynein-dependent retrograde transport in MN axons. Scale bar: 20µm.
1171
1172 **Movie 2 – Dynein-dependent retrograde transport of Lysotracker and Mitotracker**
1173 **in MN axons is blocked by dynein inhibition.**
1174 Time-lapse image series of lysosomal (green) and mitochondrial (red) trackers after
1175 applying a dynein inhibitor. The dynein-dependent retrograde transport in MN axons
1176 was blocked. Scale bar: 20µm.
1177
1178 **Movie 3 – Retrograde transport of biotin BDNF in axons of HB9::GFP MNs.**
1179 Time-lapse image series of biotin BDNF, showing retrograde transport in HB9::GFP
1180 axons. Scale bar: 20µm.
1181

1182 **Movie 4 – Retrograde transport process of biotin BDNF in axons of HB9::GFP**
1183 **MN is blocked by applying Dynasore (an endocytosis inhibitor) in the distal**
1184 **compartment of an MFC device.**
1185 Time-lapse image series of biotin BDNF after applying Dynosaore, an endocytosis
1186 inhibitor. The clathrin-dependent endocytosis event of BDNF was blocked; therefore,
1187 biotin BDNF did not undergo retrograde transport. Scale bar: 20μm.
1188

Figure 1

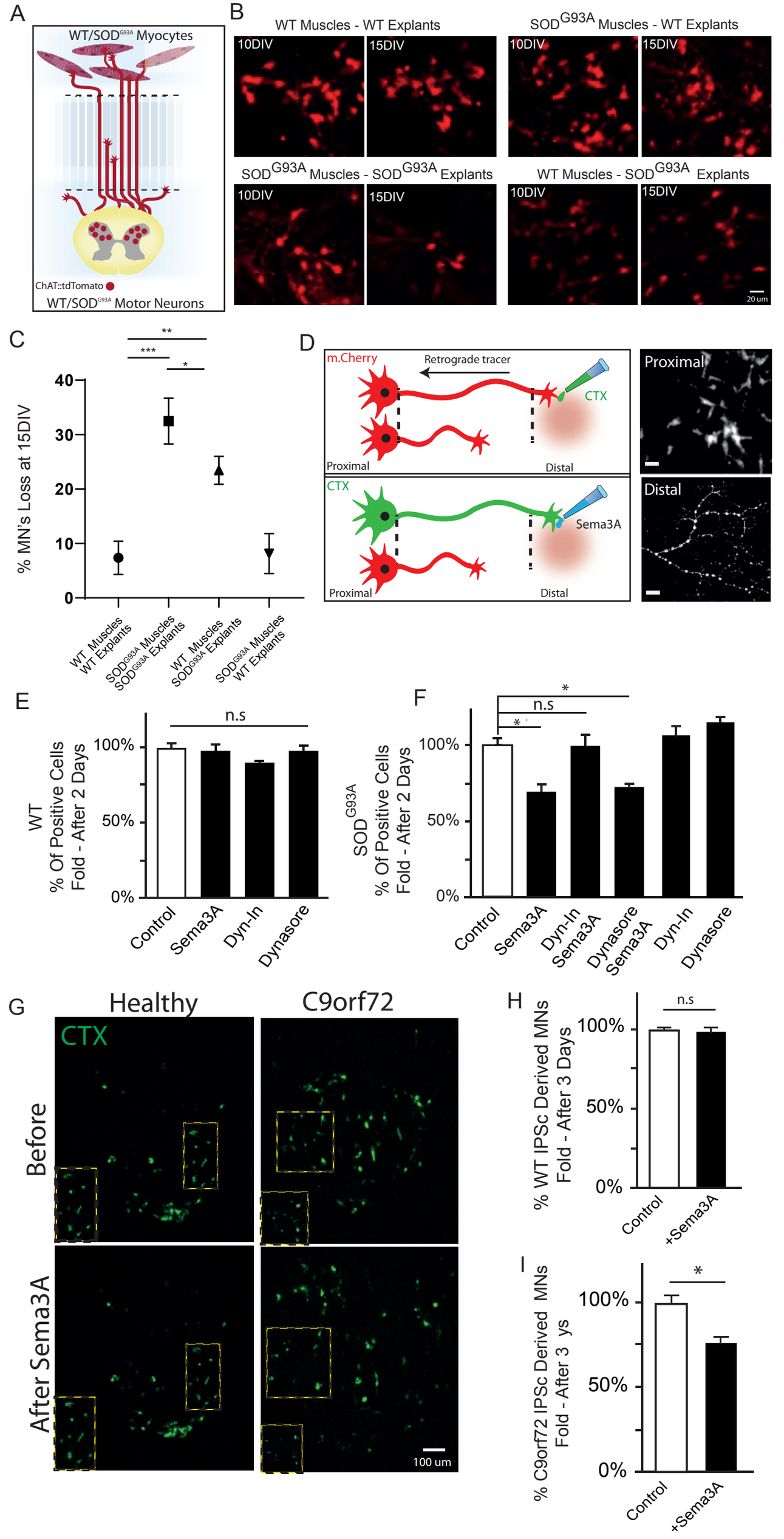
A
WT/SOD^{G93A} Myocytes
ChAT::tdTomato
WT/SOD^{G93A} Motor Neurons
B
WT Muscles - WT Explants
SOD^{G93A} Muscles - WT Explants
SOD^{G93A} Muscles - SOD^{G93A} Explants
WT Muscles - SOD^{G93A} Explants
10DIV
15DIV
20 um
C
% MN's Loss at 15DIV
WT Muscles WT Explants
SOD^{G93A} Muscles SOD^{G93A} Explants
WT Muscles SOD^{G93A} Explants
SOD^{G93A} Muscles WT Explants
D
m.Cherry
Retrograde tracer
CTX
Proximal
Distal
Sema3A
Proximal
Distal
E
WT % Of Positive Cells Fold - After 2 Days
n.s
Control
Sema3A
Dyn-In
Dynasore
F
SOD^{G93A} % Of Positive Cells Fold - After 2 Days
n.s
Control
Sema3A
Dyn-In Sema3A
Dynasore Sema3A
Dyn-In
Dynasore
G
Healthy
C9orf72
CTX
Before
After Sema3A
100 um
H
% WT IPSc Derived MNs Fold - After 3 Days
n.s
Control
+Sema3A
I
% C9orf72 IPSc Derived MNs Fold - After 3 ys
Control
+Sema3A

Figure 2

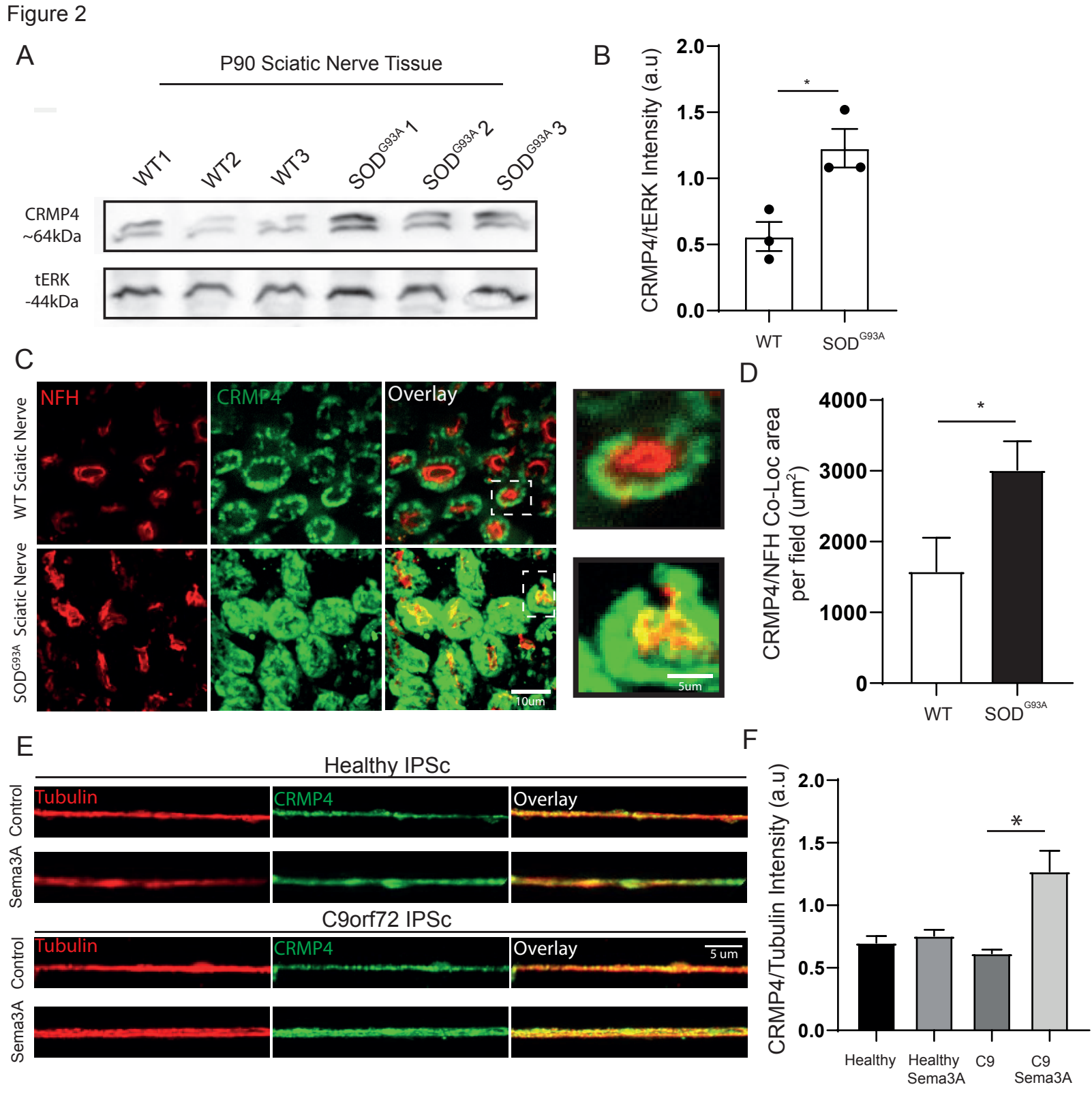
A
P90 Sciatic Nerve Tissue
WT1
WT2
WT3
SOD G93A 1
SOD G93A 2
SOD G93A 3
CRMP4
~64kDa
tERK
-44kDa
B
CRMP4/tERK Intensity (a.u)
2.0
1.5
1.0
0.5
0.0
*
WT
SOD G93A
C
NFH
CRMP4
Overlay
WT Sciatic Nerve
SOD G93A Sciatic Nerve
10um
5um
D
CRMP4/NFH Co-Loc area per field (um2)
4000
3000
2000
1000
0
*
WT
SOD G93A
E
Healthy IPSc
Control
Sema3A
Tubulin
CRMP4
Overlay
C9orf72 IPSc
5 um
F
CRMP4/Tubulin Intensity (a.u)
2.0
1.5
1.0
0.5
0.0
*
Healthy
Healthy Sema3A
C9
C9 Sema3A

Figure 3

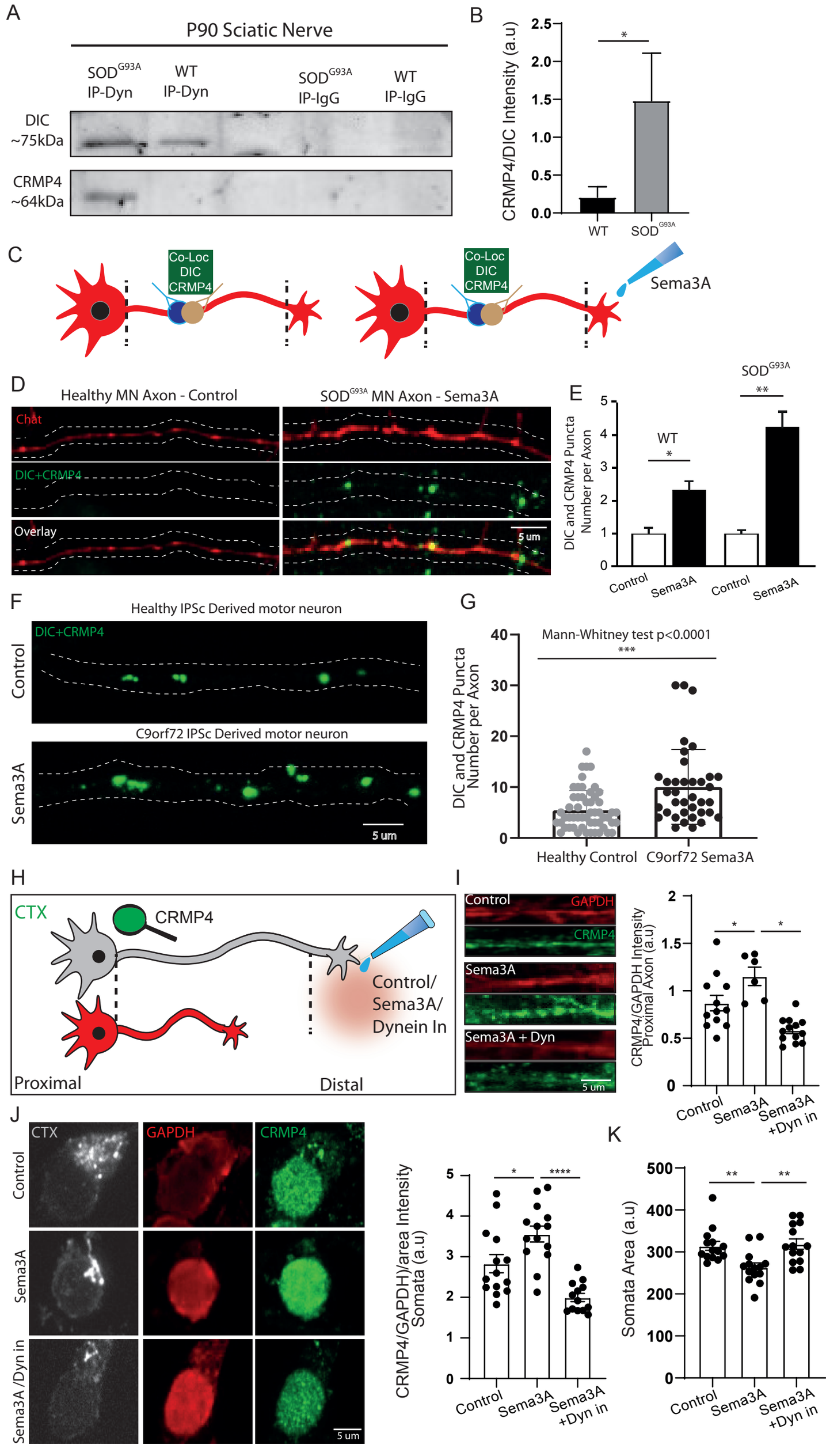
A
P90 Sciatic Nerve
SOD G93A IP-Dyn
WT IP-Dyn
SOD G93A IP-IgG
WT IP-IgG
DIC ~75kDa
CRMP4 ~64kDa
B
CRMP4/DIC Intensity (a.u)
2.5
2.0
1.5
1.0
0.5
0.0
*
WT
SOD G93A
C
Co-Loc DIC CRMP4
Co-Loc DIC CRMP4
Sema3A
D
Healthy MN Axon - Control
SOD G93A MN Axon - Sema3A
Chat
DIC+CRMP4
Overlay
5 um
E
SOD G93A
**
WT
*
DIC and CRMP4 Puncta Number per Axon
5
4
3
2
1
0
Control
Sema3A
Control
Sema3A
F
Healthy IPSc Derived motor neuron
DIC+CRMP4
Control
C9orf72 IPSc Derived motor neuron
Sema3A
5 um
G
Mann-Whitney test p<0.0001
***
DIC and CRMP4 Puncta Number per Axon
40
30
20
10
0
Healthy Control
C9orf72 Sema3A
H
CTX
CRMP4
Control/ Sema3A/ Dynein In
Proximal
Distal
I
Control
GAPDH
CRMP4
Sema3A
Sema3A + Dyn
5 um
CRMP4/GAPDH Intensity Proximal Axon (a.u)
2
1.5
1
0.5
0
*
*
Control
Sema3A
Sema3A +Dyn in
J
CTX
GAPDH
CRMP4
Control
Sema3A
Sema3A /Dyn in
5 um
CRMP4/GAPDH)/area Intensity Somata (a.u)
5
4
3
2
1
0
*
****
Control
Sema3A
Sema3A +Dyn in
K
Somata Area (a.u)
500
400
300
200
100
0
**
**
Control
Sema3A
Sema3A +Dyn in

Figure 4

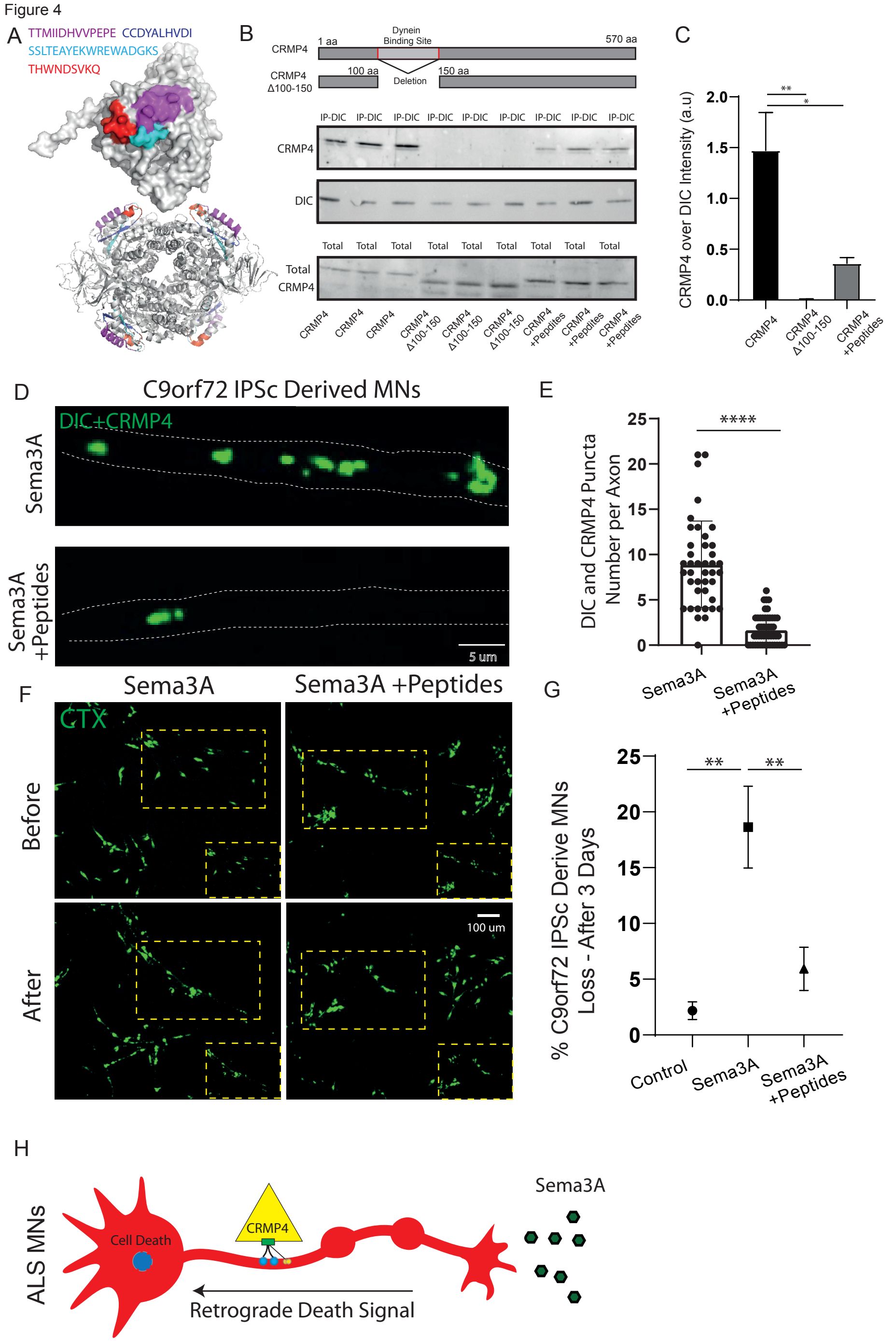
A
TTMIIDHVVPEPE CCDYALHVDI
SSLTEAYEKWREWADGKS
THWNDSVKQ
B
CRMP4
1 aa
Dynein Binding Site
570 aa
CRMP4 Δ100-150
100 aa
150 aa
Deletion
IP-DIC
CRMP4
DIC
Total
Total CRMP4
CRMP4
CRMP4 Δ100-150
CRMP4 +Pepdites
C
CRMP4 over DIC Intensity (a.u)
2.0
1.5
1.0
0.5
0.0
**
*
CRMP4
CRMP4 Δ100-150
CRMP4 +Peptides
D
C9orf72 IPSc Derived MNs
DIC+CRMP4
Sema3A
Sema3A +Peptides
5 um
E
DIC and CRMP4 Puncta Number per Axon
25
20
15
10
5
0
****
Sema3A
Sema3A +Peptides
F
Sema3A
Sema3A +Peptides
CTX
Before
After
100 um
G
% C9orf72 IPSc Derive MNs Loss - After 3 Days
25
20
15
10
5
0
**
**
Control
Sema3A
Sema3A +Peptides
H
ALS MNs
Cell Death
CRMP4
Sema3A
Retrograde Death Signal

Supplementary figure 1

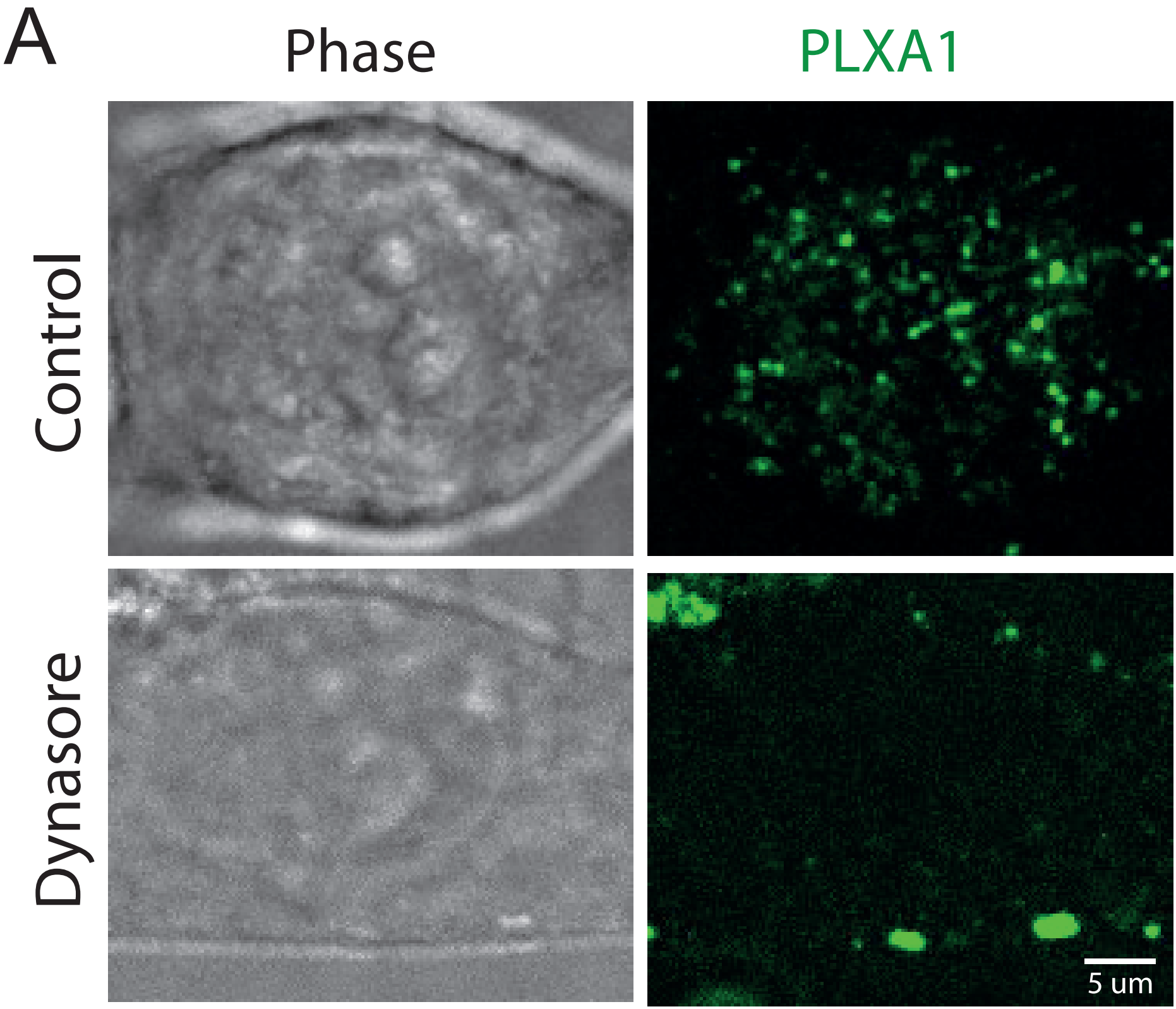

Supplementary figure 2

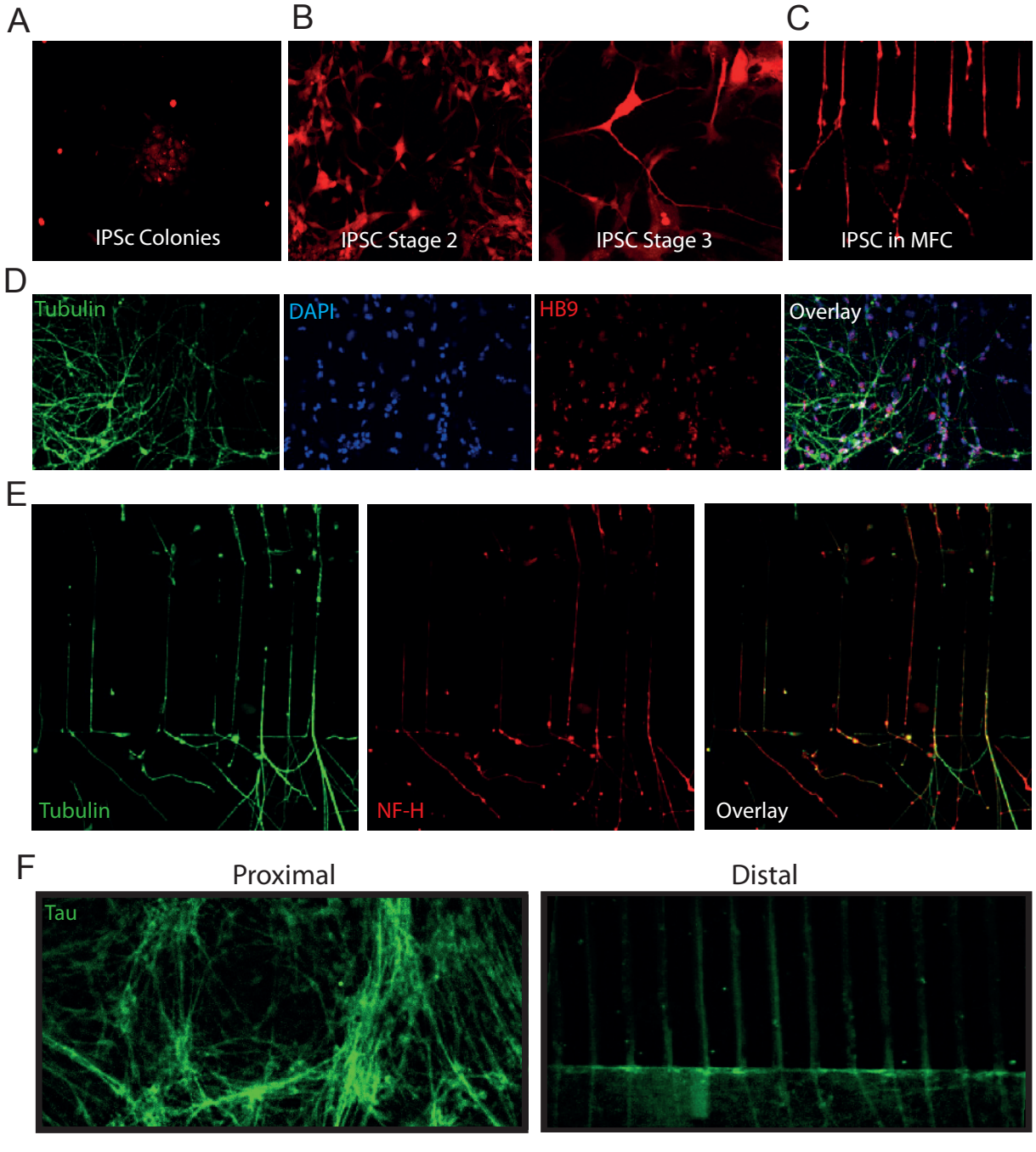
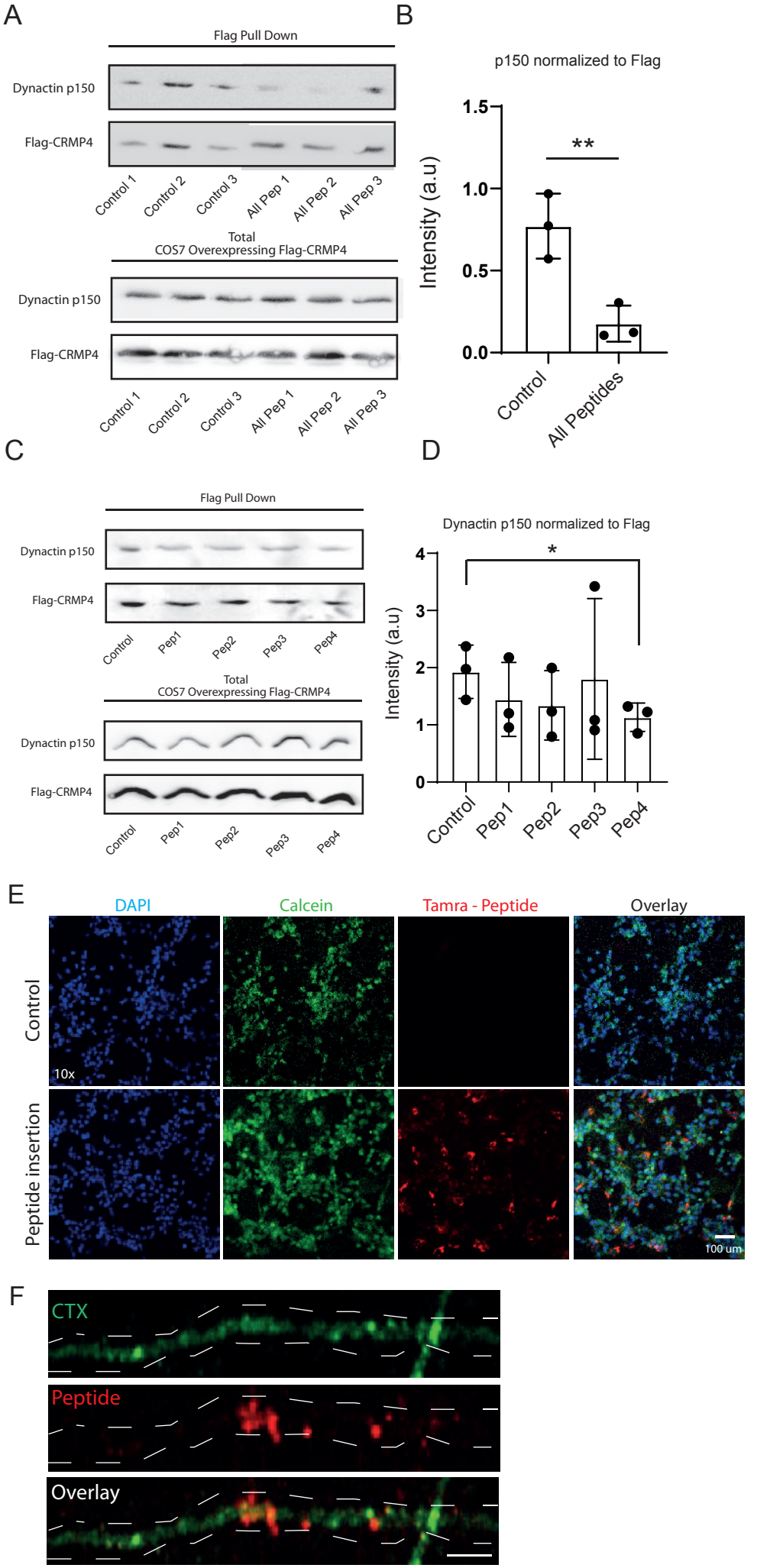
Supplementary figure 3